Supplementary Information

A 14-Vertex Bud-Shaped $[(Cp^*Ti)_2B_{12}H_{18}]$ Cluster

Subhash Bairagi,‡ Debipada Chatterjee,‡ Deepak Kumar Patel, Swetashree Acharya and Sundargopal Ghosh*

Department of Chemistry, Indian Institute of Technology Madras, Chennai 600036, India, E-mail: sghosh@iitm.ac.in

‡These authors contributed equally to this work.

Table of contents

I Experimental Details

General Procedures and Instrumentation. All manipulations were performed under an Ar/N_2 atmosphere using standard Schlenk techniques or in a glove box. Hexane, THF, and toluene were purified by distillation from benzophenone ketyl (purple solutions). Dichloromethane and $CDCl_3$ were distilled from calcium hydride prior to use. [Cp*$TiCl_3$][1] was prepared according to the reported procedure, whereas $LiBH_4$ (2.0 M in THF) and [BH_3·SMe_2] were used as received (Sigma Aldrich). Thin-layer chromatography (TLC) was carried out on 250-μm aluminum-supported silica gel plates (MERCK) for separation of reaction mixtures. NMR spectra were recorded on a Bruker Avance III 500 MHz spectrometer. Residual solvent signals ($CDCl_3$: δ = 7.26 ppm for ^{1}H and δ = 77.1 ppm for ^{13}C) were used as internal references. The ^{11}B decoupled ^{1}H spectra were acquired using inverse-gated (zgig) and power-gated (zgpr) decoupling pulse sequences. Mass spectrometric measurements were performed on a Waters Synapt G2Si HDMS system. Infrared spectra of were recorded using a JASCO FT/IR-1400 spectrometer. UV-vis spectra in CH_2Cl_2 were obtained on a Thermo Scientific Evolution 300 spectrophotometer.

Synthesis of 1-3. In a flame-dried Schlenk tube, [(Cp*$TiCl_3$] (0.100 g, 0.35 mmol) was suspended in 10 mL of dry toluene and cooled to -78 °C. Then, a 2.0 M solution of $LiBH_4$ in THF (0.6 mL, 1.2 mmol) was added dropwise, and the mixture was stirred for 1 h to generate the intermediate species. Subsequently, an excess of [BH_3·SMe_2] (2.0 mL, 2.0 mmol) was added, and the reaction mixture was heated at 100 °C for 48 h under continuous stirring. Upon addition of [BH_3·SM_2], the suspension turned light green, gradually transitioning to brown during thermolysis and finally becoming dark brown after 48 h. After completion, the solvent was removed under reduced pressure. The residue was extracted through a Celite (3 cm) frit using a hexane/dichloromethane mixture (80:20 v/v). The combined filtrate was concentrated, and the residue was purified by chromatography on 250-μm aluminium-supported silica gel TLC plates. Elution with hexane/dichloromethane (80:20 v/v) yielded violet **1** (0.015 g, 17%; R_f = 0.82), Orange **2** (0.008 g, 8%; R_f = 0.45), orange **3** in very low yield, and the previously reported 16-vertex cluster [(Cp*$Ti)_2B_{14}H_{18}$] (**III**) (0.013 g, 14%; R_f = 0.36).

Note that the crystallographic data indicates a mixture of compound **1** and a second compound with the assumed empirical formula [(Cp*$Ti)_2B_{14}H_{22}$]. However, mass spectrometry and the ^{11}B and ^{1}H NMR spectra indicate only compound **1** in solution. The ^{11}B spectrum shows only the resonances of compound **1**, with no indication of additional boron-containing impurities. The ^{1}H NMR spectrum does show a minor, inseparable impurity; however, this is not attributable to [(Cp*$Ti)_2B_{14}H_{22}$], as no additional Cp* proton signals are observed. Despite several attempts, separation or characterization of the putative [(Cp*$Ti)_2B_{14}H_{22}$] compound was unsuccessful; accordingly, no further spectroscopic discussion is included.

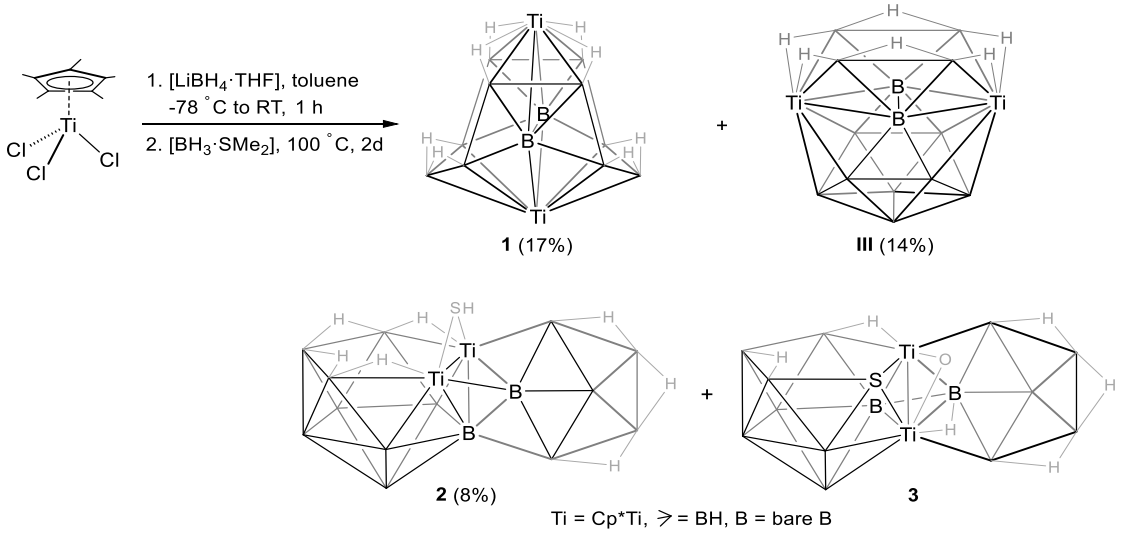

Scheme S1. Synthesis of **1**-**3**.

1: **MS (ESI$^+$)**: *m/z* calculated for $[C_{20}H_{48}B_{12}Ti_2]^+$: 514.3923, found: 514.3928; **^{11}B{^{1}H} NMR** (160 MHz, $CDCl_3$, 22 °C): δ = 4.2 (br, 4B), 6.3 (br, 4B), 15.7 (br, 2B), 28.8 (br, 2B) ppm; **^{11}B NMR** (160 MHz, $CDCl_3$, 22 °C): δ = [3.2, 3.8, 4.4, 5.0, 5.6, 6.6 (m, 8B)], 15.7 (br, 2B), 29.0 (br, 2B) ppm; **^{1}H NMR** (500 MHz, $CDCl_3$, 22 °C): δ = -6.44 (br, 4H, Ti-*H*-B), -2.28 (br, 4H, B-*H*-B), 1.92 (s, 15H, 1Cp*), 2.32 (s, 15H, 1Cp*) ppm; **^{1}H{^{11}B} NMR** (500 MHz, $CDCl_3$, 22 °C): δ = -6.44 (br, 4H, Ti-*H*-B), -2.28 (br, 4H, B-*H*-B), 1.92 (s, 15H, 1Cp*), 2.32 (s, 15H, 1Cp*), 3.55 (br, B-H*t*), 4.47 (br, B-H*t*) ppm; **^{13}C{^{1}H} NMR** (125 MHz, C_6D_6, 22 °C): δ = 13.4 and 13.5 (C_5Me_5), 119.2 and 124.8 (C_5Me_5), ppm; **IR** (cm^{-1}): $\bar{\upsilon}$ = = 2958, 2923, 2853, 2522 (B-H_t), 2133 (Ti-H_b-B), 1948 (B-H_b-B), 1743, 1459, 1379, 1259, 1094, 1028, 798, 680; **UV-Vis** (CH_2Cl_2): λ = 229,285, 430, 550 nm.

2: **MS (ESI$^+$)**: *m/z* calculated for $[C_{20}H_{51}B_{15}STi_2 - H]^+$: 580.4116, found: 580.3997; **^{11}B{^{1}H} NMR** (160 MHz, $CDCl_3$, 22 °C): δ = -49.9, -19.4, 9.9, 12.3, 14.3, 25.4, 27.4, 30.5, 32.8, 39.7 ppm; **^{11}B NMR** (160 MHz, $CDCl_3$, 22 °C): δ = [-50.6 and -49.3 (d, $^1J_{B\text{-}H}$ = 154 Hz)], [-20.1 and -18.9 (d, $^1J_{B\text{-}H}$ = 158 Hz)], 9.7 (br), 13.6 (br), 14.8 (br), 25.0 (br), 27.3 (br), [30.0 and 30.9 (d, $^1J_{B\text{-}H}$ = 120 Hz)], 32.7 (br), [39.2 and 40.0 (d, $^1J_{B\text{-}H}$ = 103 Hz)] ppm; **^{1}H NMR** (500 MHz, $CDCl_3$, 22 °C): δ = -2.71 (br, 2H, Ti-*H*-B), -1.99 (br, 1H, B-*H*-B), -1.27 (br, 2H, B-*H*-B), -0.26 (br, 2H, B-*H*-B), 1.97 (s, 15H, 1Cp*), 2.03 (s, 15H, 1Cp*) ppm; **^{1}H{^{11}B} NMR** (500 MHz, $CDCl_3$, 22 °C): δ = -2.71 (br, 2H, Ti-*H*-B), -2.00 (br, 1H, B-*H*-B), -1.27 (br, 2H, B-*H*-B), -0.26 (br, 2H, B-*H*-B), 1.97 (s, 15H, 1Cp*), 2.03 (s, 15H, 1Cp*), 2.87 (br, B-H*t*), 3.35 (br, B-H*t*), 3.49 (br, B-H*t*), 4.45 (br, B-H*t*) ppm; **^{13}C{^{1}H} NMR** (125 MHz, $CDCl_3$, 22 °C): δ = 13.1 and 14.3 (C_5Me_5), 125.7 and 126.5 (C_5Me_5), ppm; **IR** (cm^{-1}): $\bar{\upsilon}$ = = 2955, 2923, 2853, 2597 (S-H), 2539 (B-H_t), 2481 (B-H_t), 1746, 1462, 1376, 1259, 1092, 1022, 862, 801, 699; **UV-Vis** (CH_2Cl_2): λ = 220,256, 370, 520 nm.

Compound **3**, which is structurally similar to **2**, was also isolated from the same reaction mixture. However, due to its poor yield and lack of reproducibility, we were unable to fully characterize this unusual cluster beyond X-ray diffraction studies. Therefore, we are unable to provide any spectroscopic details for compound **3**.

Assignment of the bridging hydrogens in 1: The X-ray structure of cluster **1** reveals 10 terminal B–H hydrogens. However, the isotopic pattern observed in the mass spectrum corresponds to the molecular formula $[(Cp^*Ti)_2B_{12}H_{18}]$, indicating the presence of eight bridging hydrogens that could not be located crystallographically. The ^{1}H NMR spectrum shows two upfield resonances at δ = −2.28 and −6.42 ppm in a 1:1 ratio that corresponds to B–H–B and Ti–H–B bridging hydrogens, respectively. This indicates the presence of four Ti–H–B and four B–H–B bridging hydrogens. Structurally, the four Ti–H–B hydrogens are most reasonably associated with the Ti1 center, which is a degree-six vertex located at an open face of the cluster, whereas Ti2 is a degree-eight vertex positioned at a closed face.

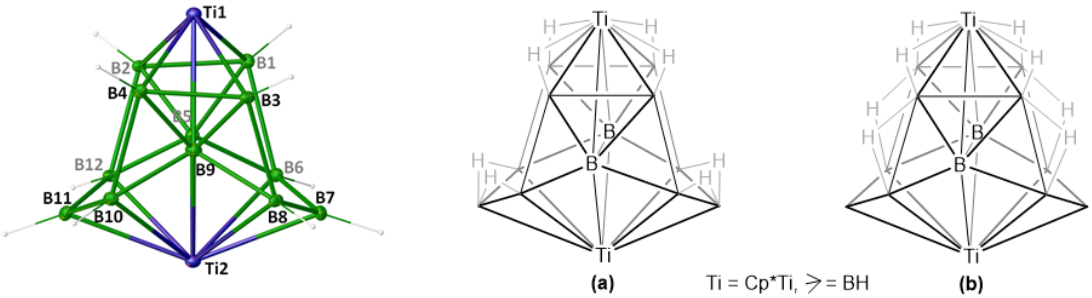

Figure S1. (Left) Molecular structure and atom-labelling diagram of **1**. The Cp* ligands attached to Ti atoms are omitted for clarity. The eight bridging hydrogen atoms could not be located crystallographically. (Middle and right) Two possible arrangements (a) and (b) for the B–H–B bridging hydrogens.

For the B–H–B bridging hydrogens, two possible arrangements (a) and (b) can be considered. The ^{11}B{^{1}H} NMR spectrum exhibits four resonances at δ = 4.2, 6.3, 15.7, and 28.8 ppm in a 4:4:2:2 ratio. In the ^{11}B NMR spectrum (proton

coupled), the signals at δ = 4.2 and 6.3 ppm appear as approximate doublets of doublets, δ = 15.7 ppm shows no significant change, and δ = 28.8 ppm appears broadened. Based on the intensity ratio and coupling patterns: the resonances at δ = 4.2 and 6.3 ppm are assigned to two sets of four boron atoms (B6, B8, B10, B12) and (B1, B2, B3, B4), respectively. Their similar chemical shifts and splitting patterns indicate comparable environments. This is consistent with arrangement (a), where each of these boron atoms bears one terminal and one bridging hydrogen. In contrast, arrangement (b) would generate distinctly different environments: one set would have one terminal and one bridging hydrogen, while the other would have one terminal and two bridging hydrogens, which should lead to noticeably different chemical shifts and splitting patterns. This is not the case observed experimentally. The resonance at δ = 28.8 ppm is assigned to B5 and B9. In arrangement (a), these boron atoms are attached to one terminal and two bridging hydrogens, leading to peak broadening rather than well-resolved splitting, consistent with the experimental observation. In arrangement (b), a clear doublet would be expected, which is not observed. The resonance at δ = 15.7 ppm is assigned to boron atoms lacking any hydrogens; the absence of peak broadening in the ^{11}B NMR spectrum supports this assignment. On this basis, the experimental ^{1}H, ^{11}B{^{1}H}, and ^{11}B NMR data strongly support arrangement (a) over (b).

Furthermore, DFT geometry optimizations were performed starting from both possible hydrogen arrangements (a and b). During optimization, arrangement (b) converged to arrangement (a), which corresponds to the lowest-energy structure. The calculated chemical shifts are in good agreement with the experimental values, as shown in the table below.

Table S1. Correlation between experimental and calculated chemical shifts of **1**.

	Atomic positions	Experimental	Calculated
^{11}B NMR (ppm)	B1, B2, B3, B4	4.2 (or 6.3)	3.5, 3.6, 7.3, 7.4
	B6, B8, B10, B12	6.3 (or 4.2)	4.3, 4.6, 5.2, 5.5
	B5, B9	15.7	14.4, 14.6
	B7, B11	28.8	25.2, 25.8
^{1}H NMR (ppm)	4 B–*H*–B	-2.28	-2.2, -2.3, -2.3, -2.4
	4 Ti–*H*–B	-6.44	-6.5, -6.5, -6.9, -6.9

I.1 UV-visible Studies.

To investigate the optical properties of the coloured metallaborane clusters **1** and **2**, UV-vis absorption studies were performed in CH_2Cl_2 solution. The spectra were recorded over the range 200-800 nm at 298 K (Figures S28). Both complexes exhibit intense high-energy absorptions in the 220-285 nm region, corresponding to the π–π* transitions of the Cp* ligands, which are characteristic of Cp*-based metal complexes.[2] In addition, weaker low-energy absorptions (λ>370 nm) appear as two to three distinct bands in the 370-550 nm region, attributable to charge-transfer transitions.[3,4] Time-dependent DFT (TD-DFT) calculations were carried out to reproduce the UV-vis spectra and gain insight into the nature of the electronic transitions (Figures S35 and S36, Tables S4 and S5). The calculations indicate that the absorptions observed between 370 and 550 nm arise primarily from electronic transitions involving electron-density transfer from the boron frameworks to the titanium centres.

I.2 Supplementary Data

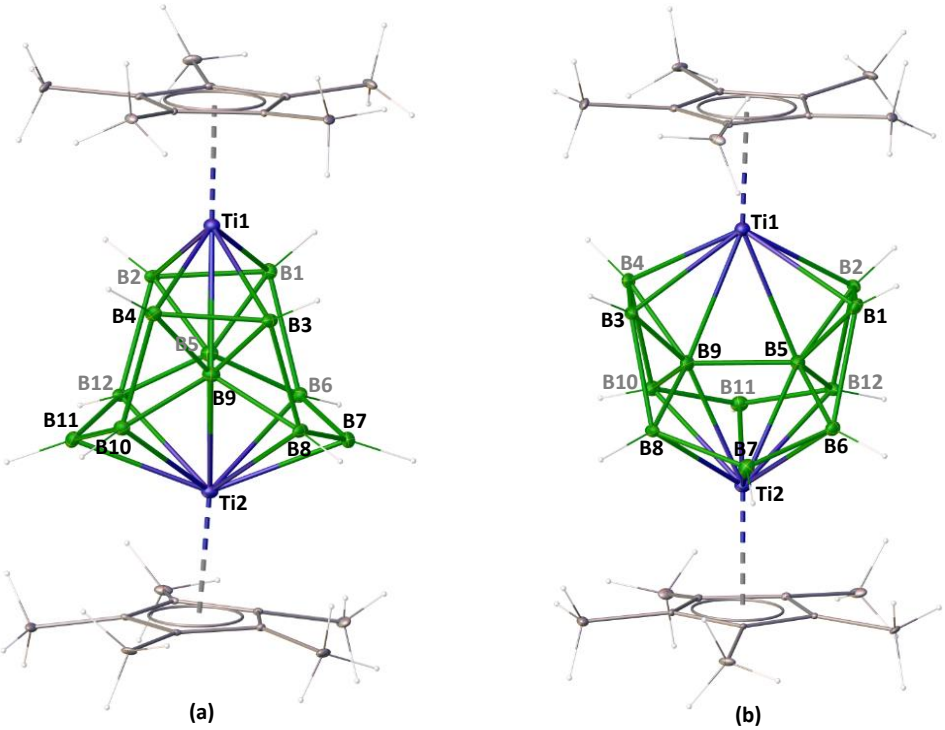

Figure S2. Molecular structure and atom-labelling diagram of **1**. (a) front view and (b) side view. The bridging hydrogen atoms could not be located crystallographically. Selected bond lengths (Å) and angles (°): Ti1−B1 2.361(6), Ti1−B5 2.329(14), Ti2−B5 2.290(14), B1−B2 1.753(11), B5−B9 1.68(2), B1−B6 2.008(10), Ti1−B9−Ti2 137.6(7), B1−Ti1−B3 108.8(3), Ti1−B5−Ti2−B9 179.57.

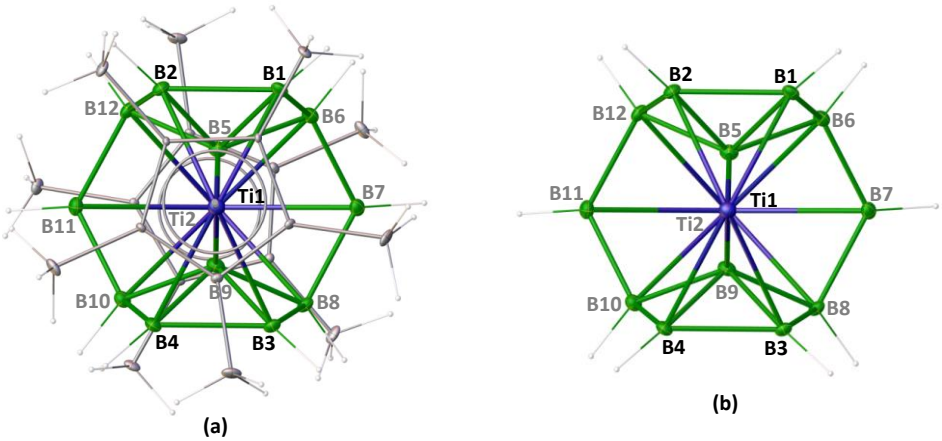

Figure S3. Molecular structure of **1** (top view). (a) with Cp* ligands and (b) without Cp* ligands.

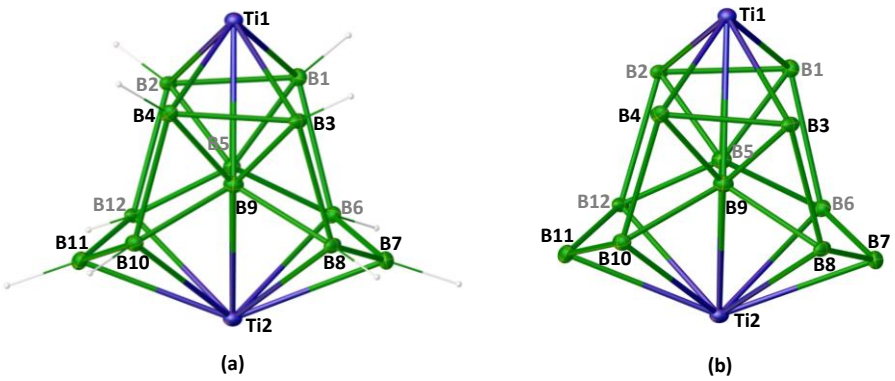

Figure S4. $[Ti_2B_{12}]$ core of cluster **1.** (a) with hydrogens and (b) without hydrogens.

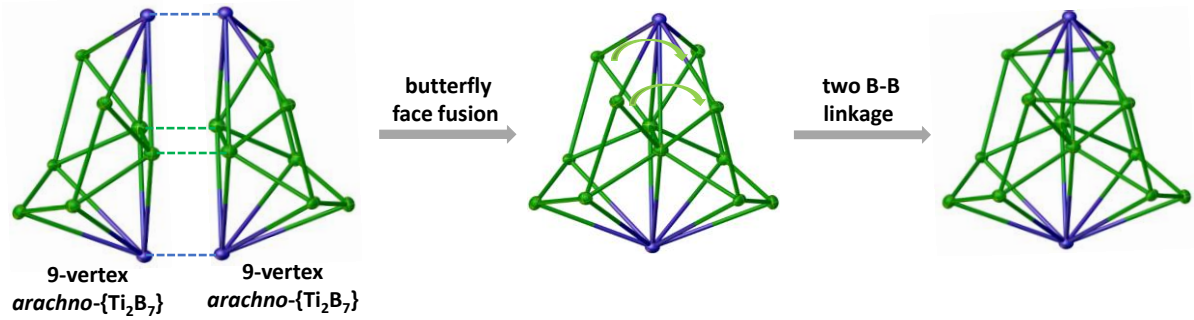

Figure S5. Schematic illustration of the generation of cluster **1** through butterfly-face fusion of two 9-vertex *arachno*-geometry, followed by the formation of two inter-subcluster B–B linkages.

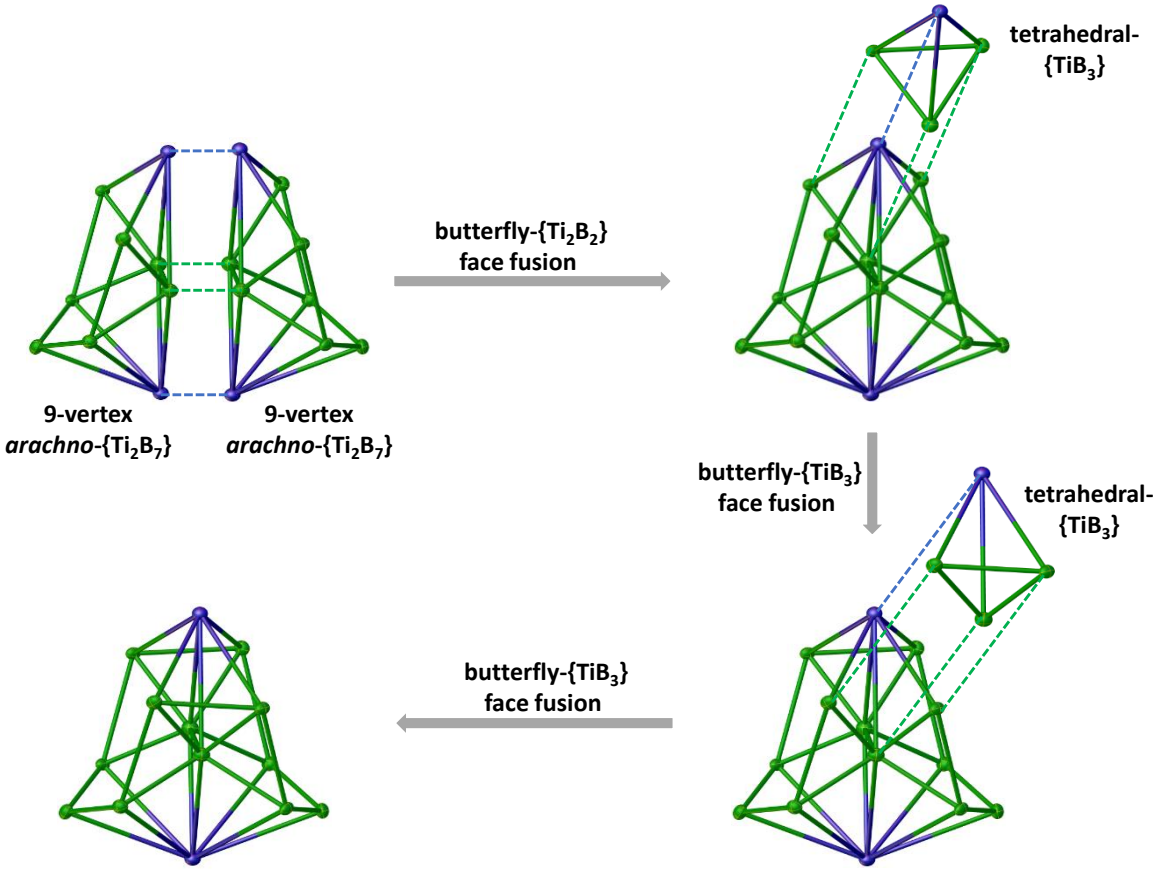

Figure S6. Schematic illustration of the generation of cluster **1** through the fusion of two *arachno*-{Ti_2B_7} and two tetrahedral-{TiB_3} cages, fused through three butterfly faces, one {Ti_2B_2} and two {TiB_3}.

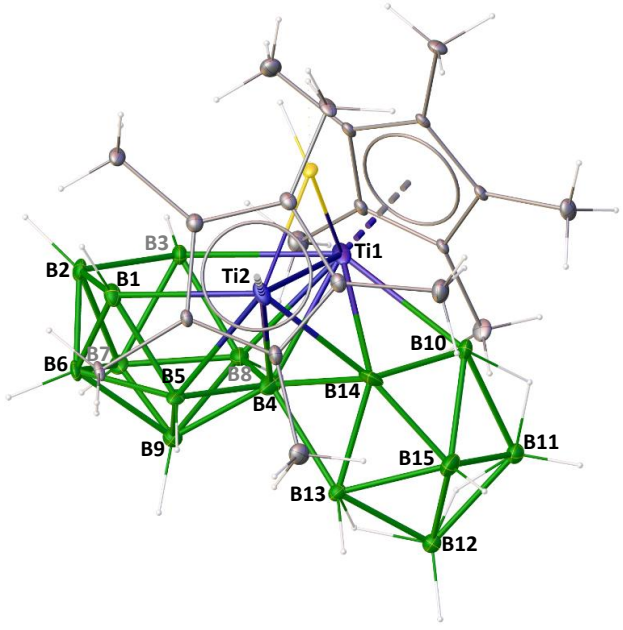

Figure S7. Molecular structure and atom-labelling diagram of **2**. Four bridging hydrogen atoms (Ti2−H−B1, B1−H−B2, B2−H−B3, and B3−H−Ti1) and the terminal B10−H hydrogen atom could not be located crystallographically. Selected bond lengths (Å) and angles (°):Ti1−Ti2 3.251(4), Ti1−B3 2.633(19), Ti1−B10 2.58(2), Ti1−B14 2.66(2), B4−B14 1.87(3), B14−B15 1.74(3), Ti1−S1 2.309(5), S1−H 1.14(3), Ti1−B10−B11 120.8(13), Ti1−S1−Ti2 91.03(15).

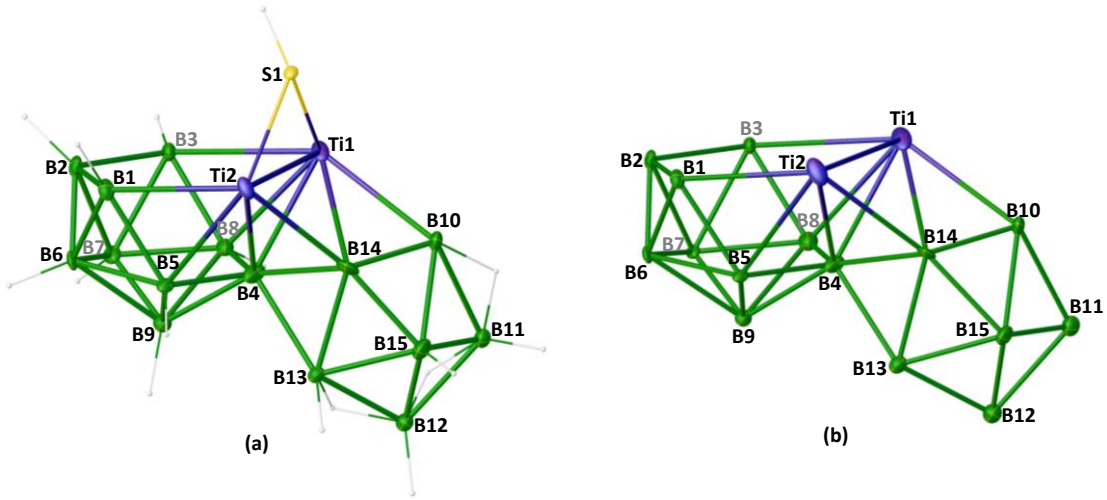

Figure S8. [Ti_2B_{15}] core of **2.** (a) with hydrogens and bridging SH group and (b) without hydrogens and bridging SH group.

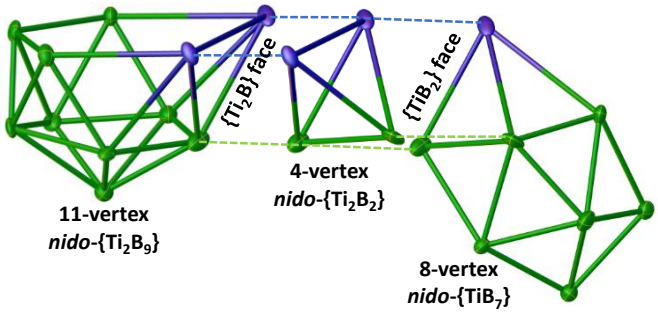

Figure S9. Representation of the fusion of three *nido*-subclusters via two shared triangular faces in **2**.

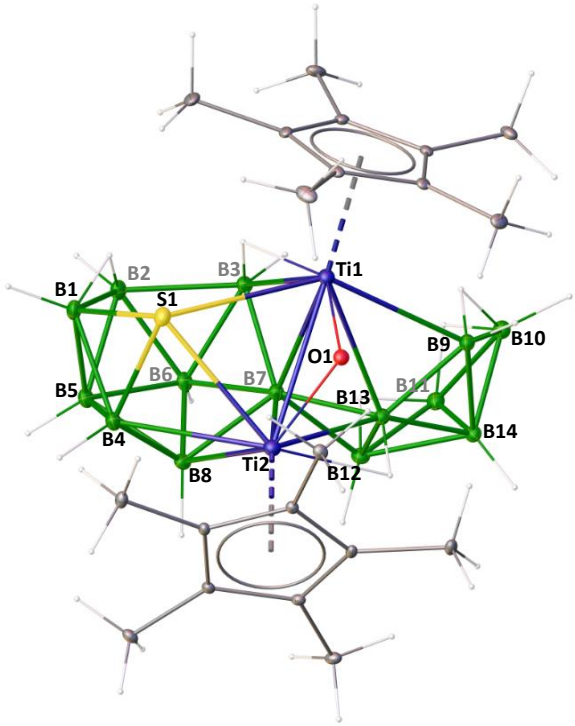

Figure S10. Molecular structure and atom labelling diagram of **3**. Selected bond lengths (Å) and angles (°):Ti1−Ti2 2.7767(9), Ti1−B3 2.555(4), Ti1−B9 2.578(4), Ti1−B13 2.506(4), Ti2−B13 2.441(4), Ti1−S1 2.6730(11), Ti1−O1 2.828(2), B1−S1 1.957(5), B2−B3 1.897(6), B13−B14 1.809(6), Ti1−S1−B1 112.25(16), Ti1−O1−Ti2 98.05(11), Ti1−B9−B10 127.2(3). Cluster **3** is structurally similar to **2**, except that one $\{BH_3\}$ unit is replaced by an {S} group and the μ-SH bridge is replaced by a μ-O bridge, with the remaining hydrogen atom forming a B-H-Ti bridge (B13-H_b-Ti2). The Ti1-Ti2 bond length in **3** (2.372 Å) is significantly shorter than that in **2** (3.376 Å). This shortening may result from the less rigid open-face environment and the presence of a bridging SH group in **2**, compared to the more rigid oxo bridge between the titanium atoms in **3**. The resulting change in the positions of the titanium centers within the cluster framework leads to different orientations of the two open *nido*-faces.

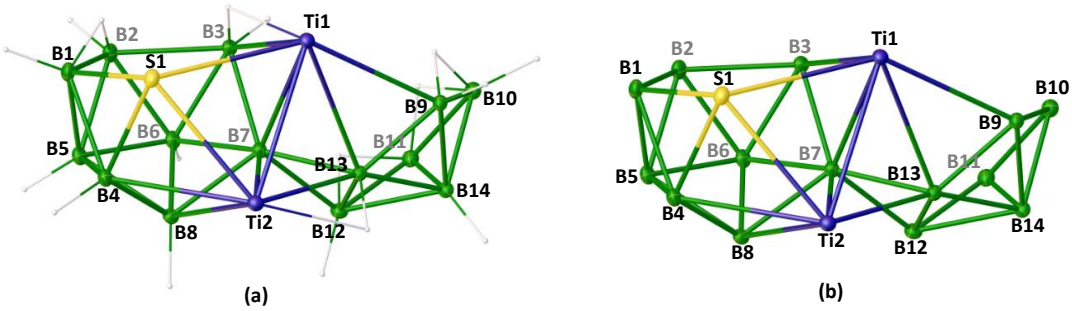

Figure S11. (a) $[Ti_2B_{14}S]$ core of cluster **3** with hydrogens and (b) without hydrogens.

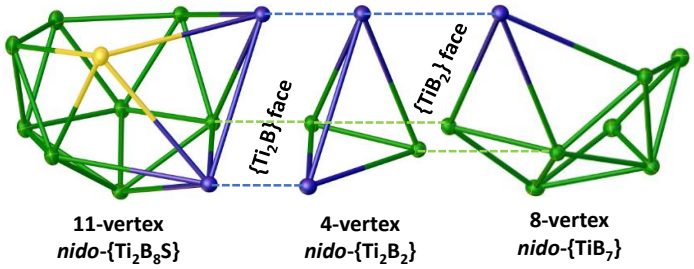

Figure S12. Representation of the fusion of three *nido*-subclusters via two shared triangular faces in **3**.

I.3 Spectroscopic Details

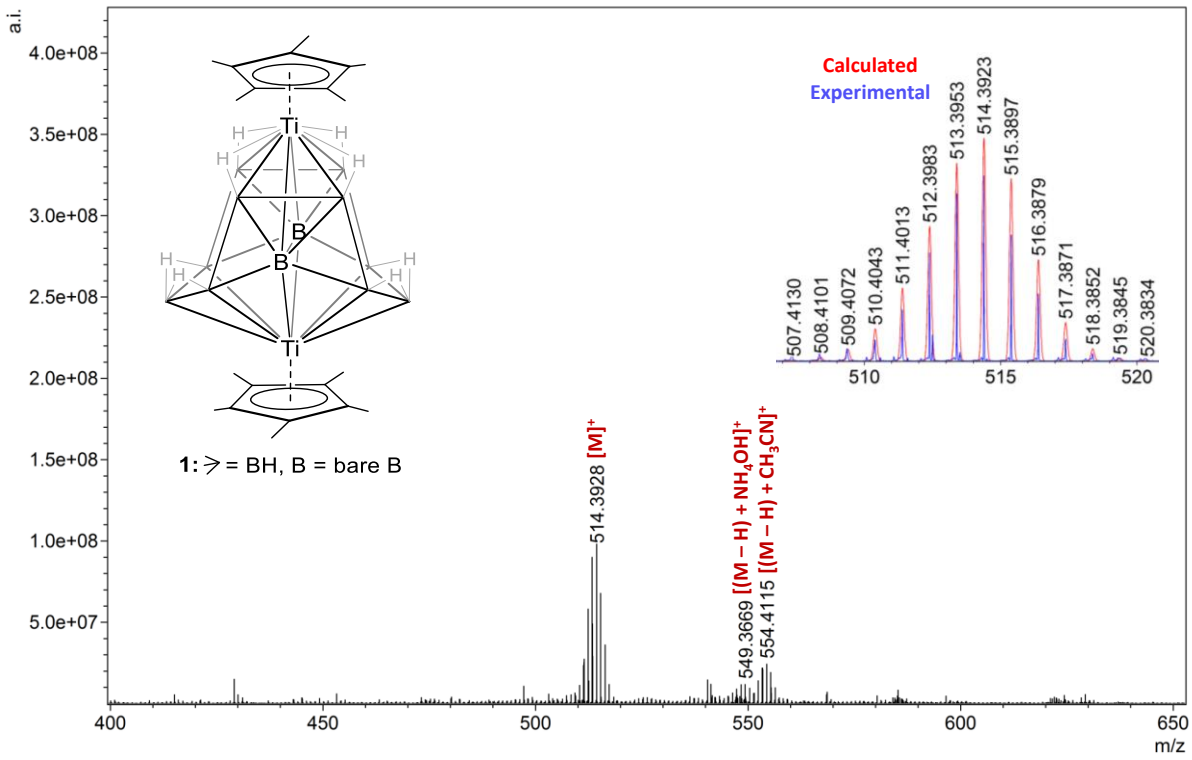

Figure S13. ESI-MS spectrum of **1**.

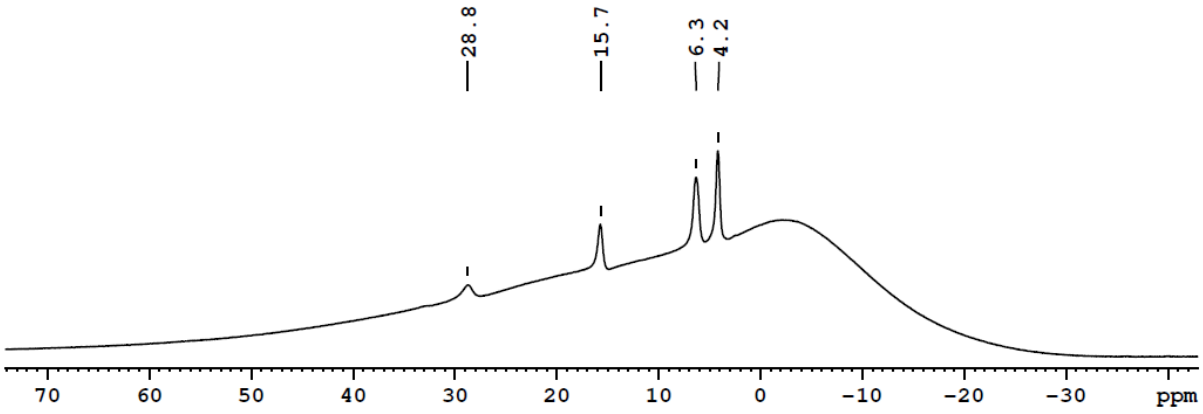

Figure S14. $^{11}B\{^{1}H\}$ NMR spectrum of **1** in $CDCl_3$.

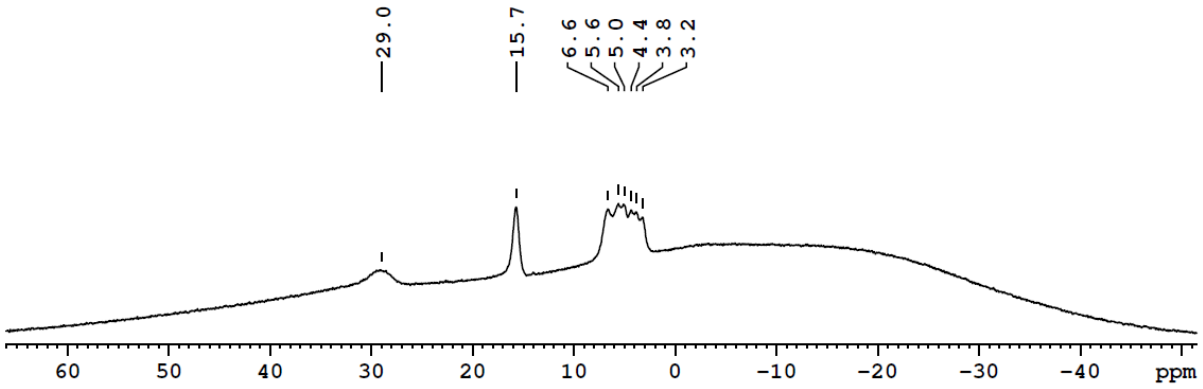

Figure S15. ^{11}B NMR spectrum of **1** in $CDCl_3$.

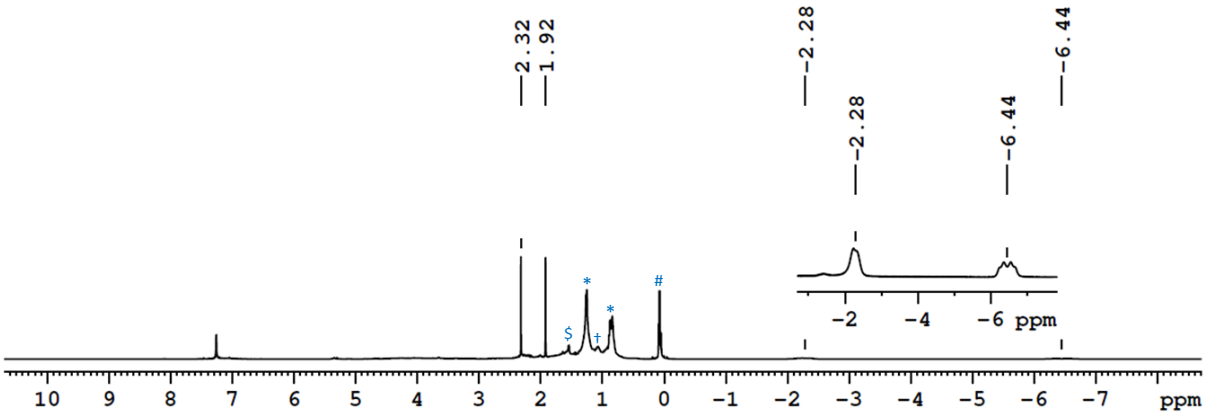

Figure S16. ^{1}H NMR spectrum of **1** in $CDCl_3$ ($H_2O, †Inseparable impurity, *Grease, #Silicon grease).

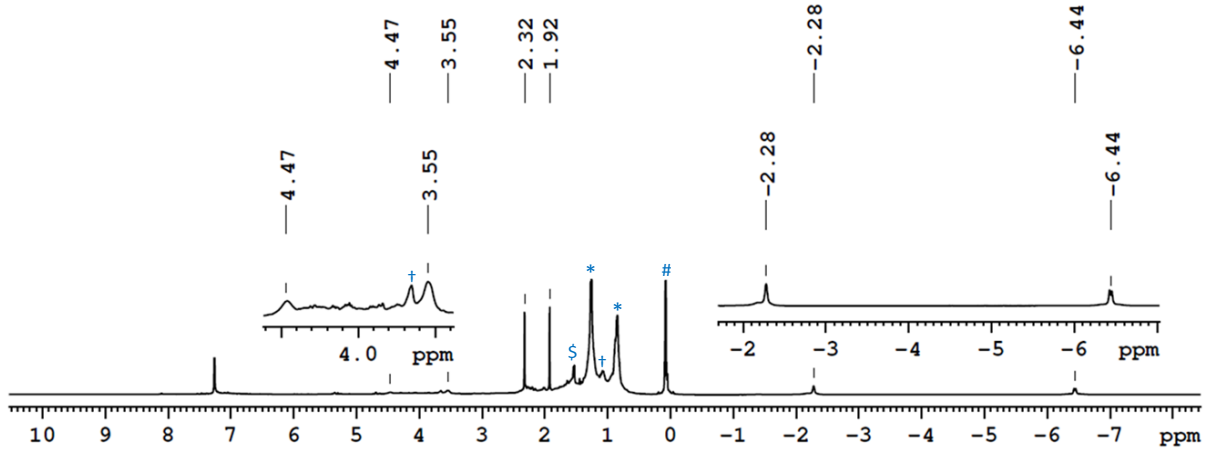

Figure S17. ^{1}H{^{11}B} NMR spectrum of **1** in $CDCl_3$ ($H_2O, †Inseparable impurity, *Grease, #Silicon grease).

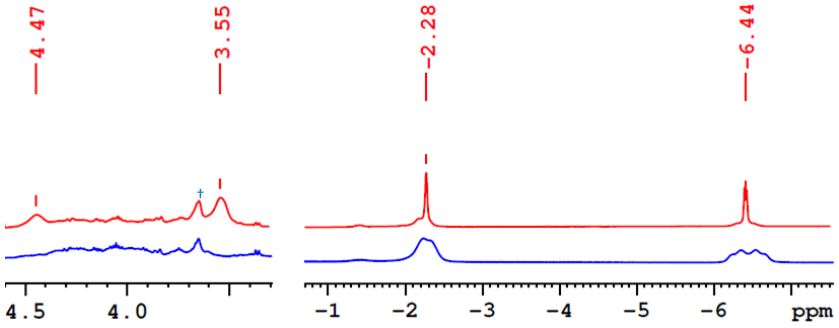

Figure S18. Stacked ^{1}H (bottom) and $^{1}H\{^{11}B\}$ NMR (top) spectra of **1** in $CDCl_3$ (†Inseparable impurity).

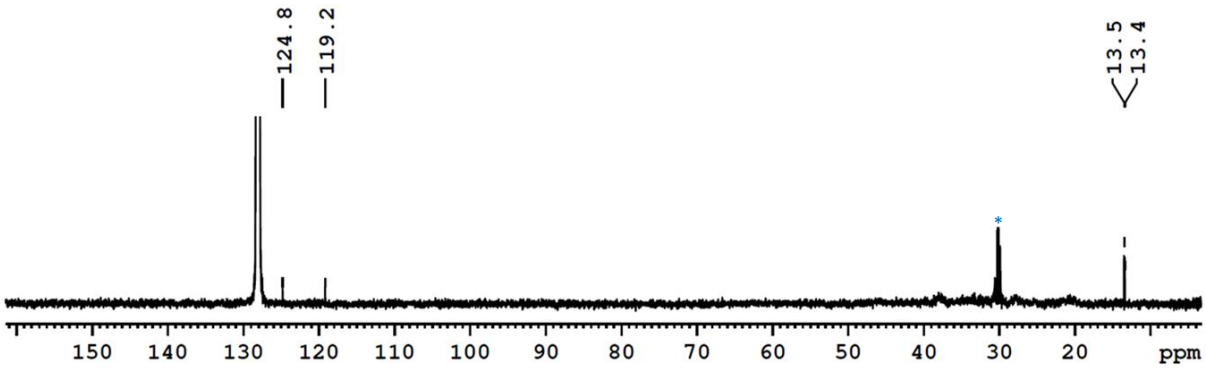

Figure S19. $^{13}C\{^{1}H\}$ NMR spectrum of **1** in C_6D_6 (*Grease).

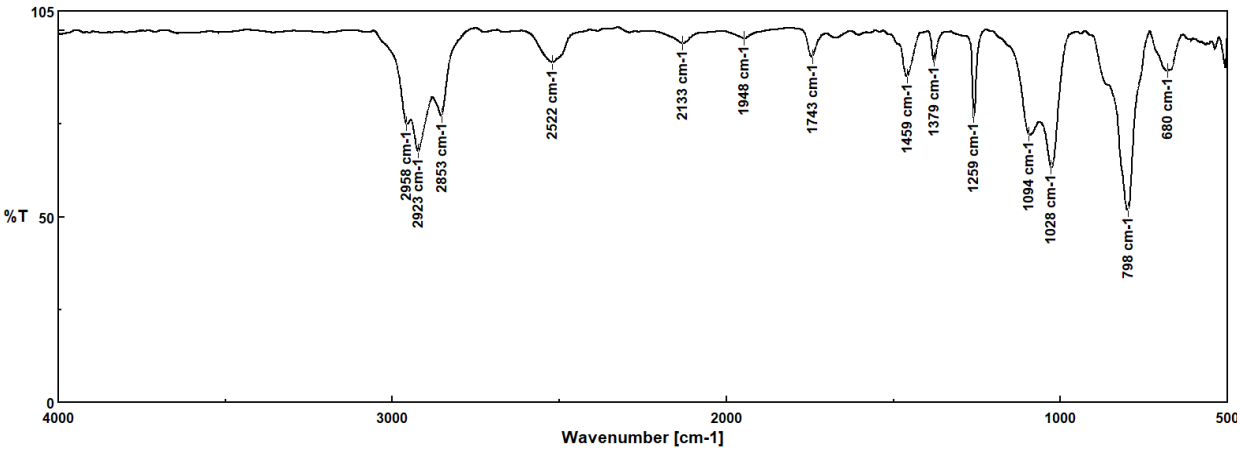

Figure S20. IR spectrum of **1**.

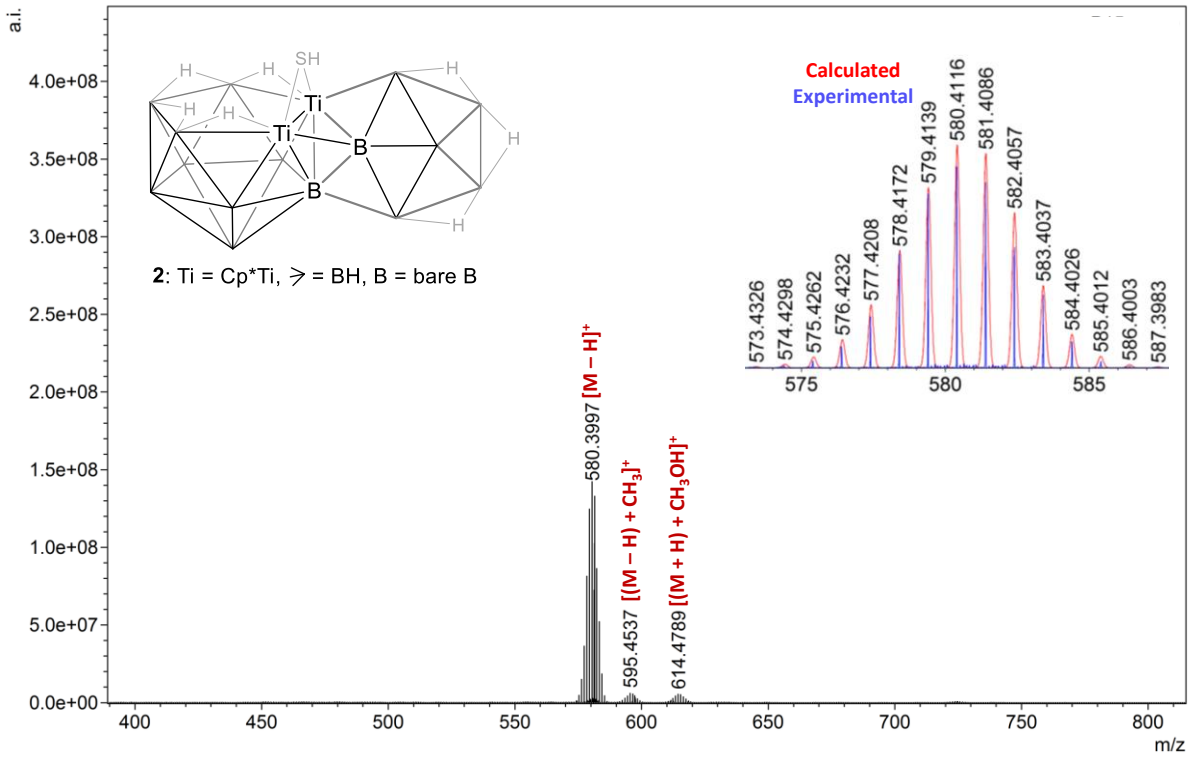

Figure S21. ESI-MS spectrum of **2**.

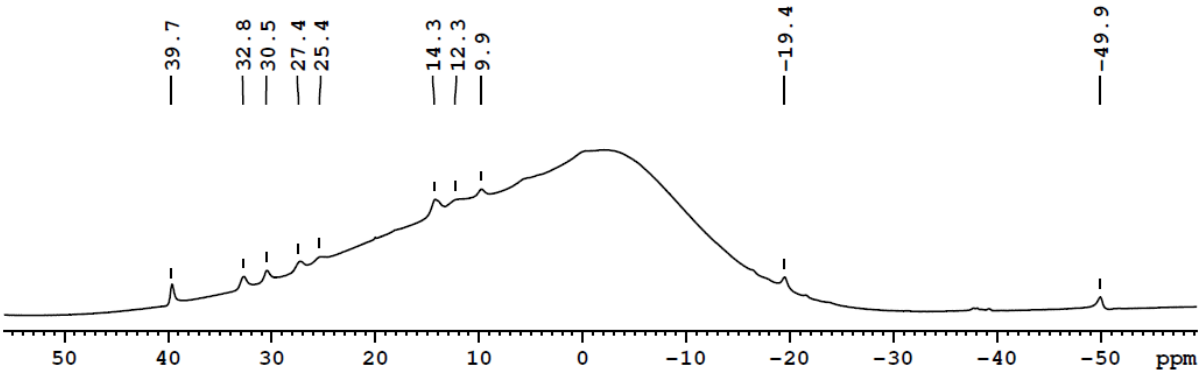

Figure S22. $^{11}B\{^{1}H\}$ NMR spectrum of **2** in $CDCl_3$.

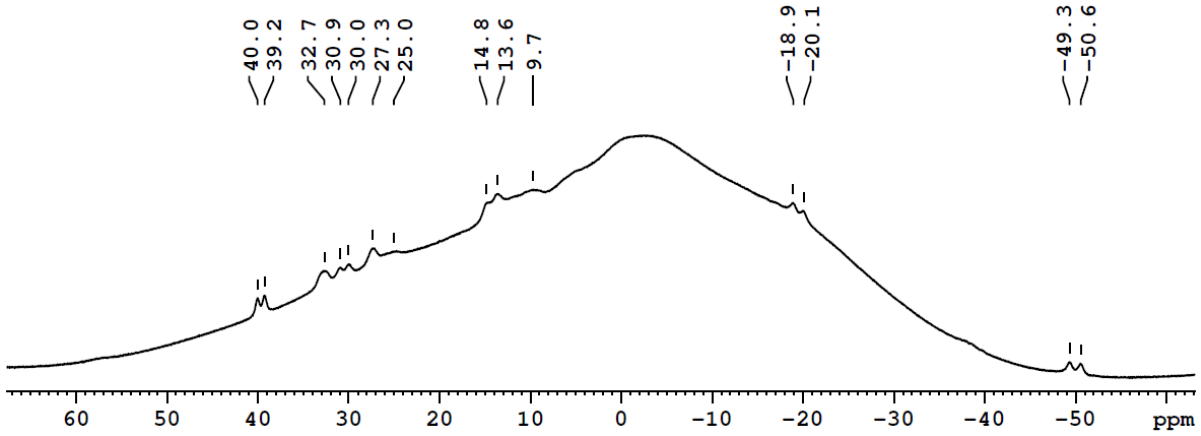

Figure S23. ^{11}B NMR spectrum of **2** in $CDCl_3$.

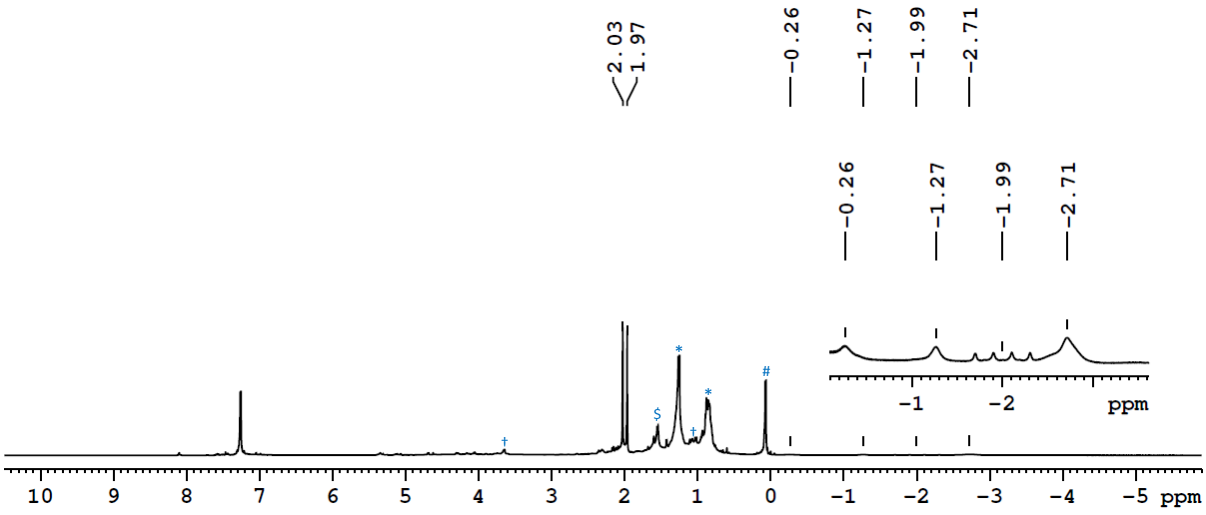

Figure S24. ^{1}H NMR spectrum of **2** in $CDCl_3$ (H_2O, †Inseparable impurity, *Grease, #Silicon grease).

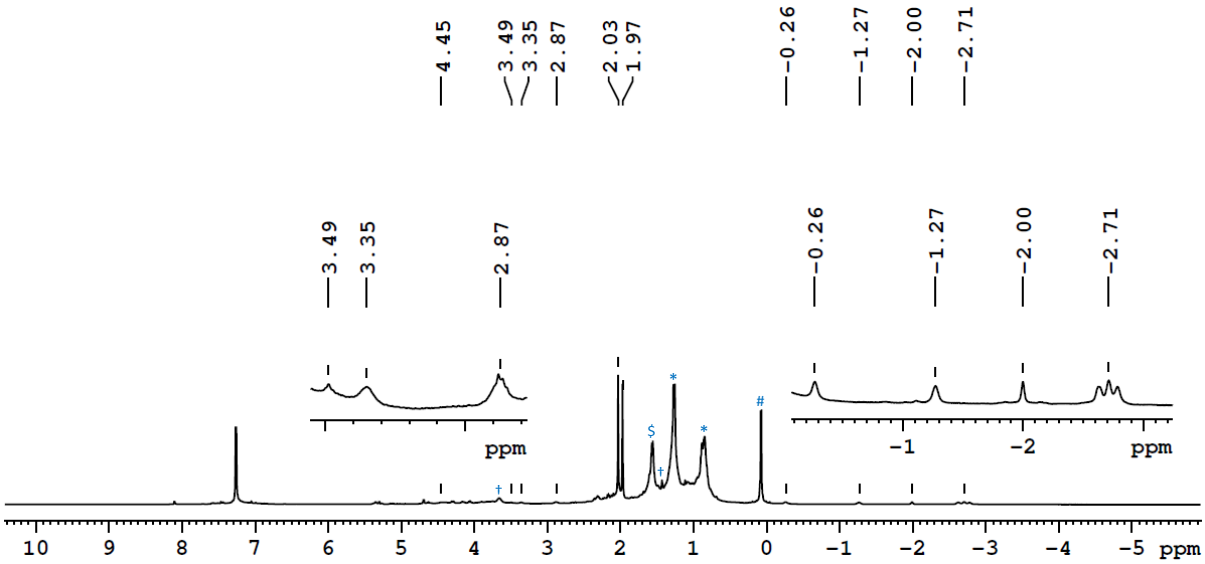

Figure S25. $^{1}H\{^{11}B\}$ NMR spectrum of **2** in $CDCl_3$ ($H_2O, †Inseparable impurity, *Grease, #Silicon grease).

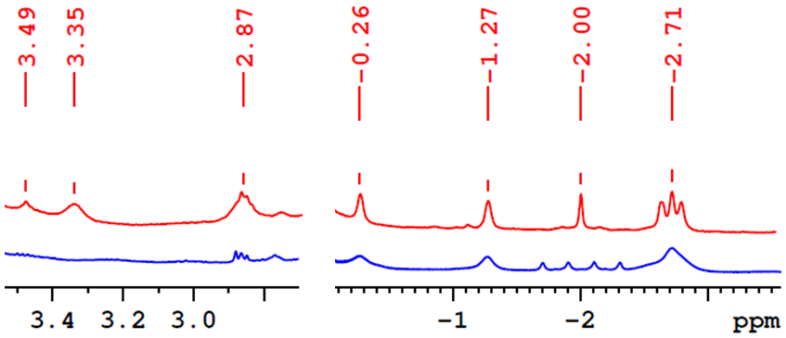

Figure S26. Stacked ^{1}H (bottom) and $^{1}H\{^{11}B\}$ NMR (top) spectra of **2** in $CDCl_3$.

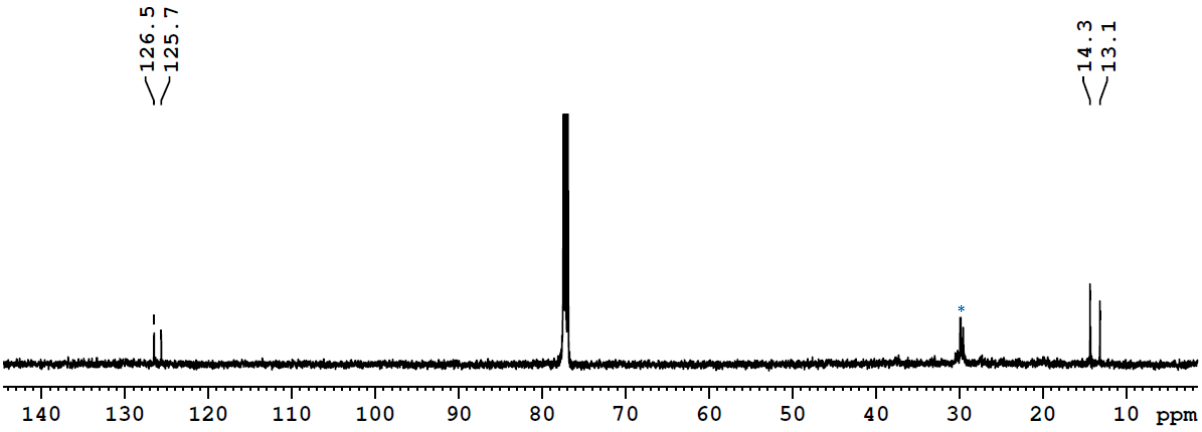

Figure S27. $^{13}C\{^{1}H\}$ NMR spectrum of **2** in $CDCl_3$ (*Grease).

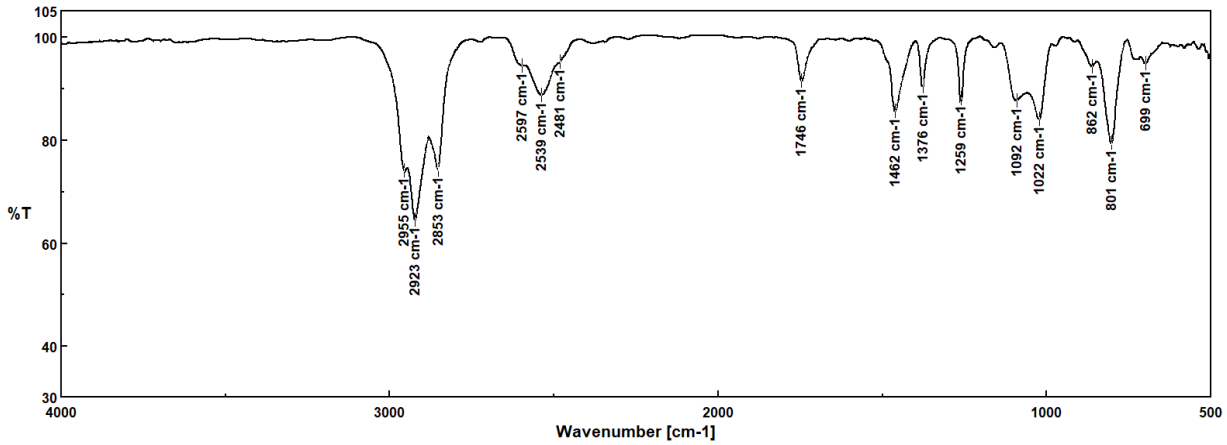

Figure S28. IR spectrum of **2**.

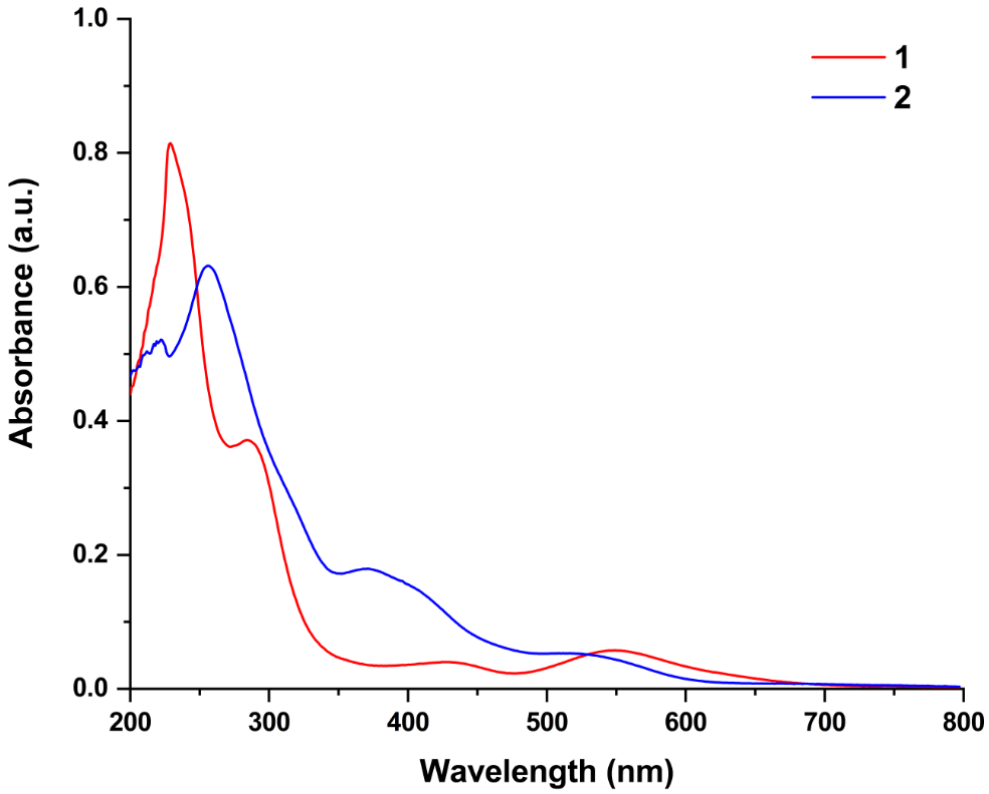

Figure S29. Combined UV-vis spectra of **1** and **2** in CH_2Cl_2.

I.4 *X-ray Analysis Details*

Single crystals suitable for X-ray diffraction analysis for **1**, **2** and **3** were obtained by slow diffusion of a hexane/dichloromethane mixture (80:20 v/v) at -5 ˚C. Crystal data for **1** and **2** were collected on a Bruker APEX3 CMOS diffractometer equipped with graphite-monochromated MoKα radiation (λ = 0.71073 Å) at 264(2) K for **1** and 298(2) K for **2**. Data for **3** were collected on a Bruker Kappa APEX2 CCD diffractometer using graphite-monochromated MoKα radiation (λ = 0.71073 Å) at 150(2) K. Structure solution was carried out using SIR92[5] and refinements were performed with SHELXL-2019/2.[6] Molecular structures were generated using Olex2.[7] Note that compound **1** crystallises in the triclinic system, space group P-1, with three independent molecules in the asymmetric unit. Each molecular unit is a disordered mixture of $[(Cp^*Ti)_2B_{12}H_{10+n}]$ and $[(Cp^*Ti)_2B_{14}H_{12+n}]$ (where *n* denotes the number of bridging hydrogens). All radial B-H hydrogen atoms, which appeared in the difference Fourier map, were fixed during refinement. The Ti-H-B and B-H-B bridging hydrogens could not be located but are included in the molecular formula. A minor B-level alert is present and addressed in the VRF section appended to the CIF. For compound **2**, the data quality was limited; the maximum Bragg angle reached only 23°. This resulted in an unavoidable A-level alert in checkCIF, which is explained in the corresponding VRF section. Hexane and dichloromethane were used for crystallisation. The difference Fourier map after refinement displayed several peaks above 1 electron/Å^3, but none could be modelled as meaningful solvent molecules. Therefore, the dataset was treated using the PLATON SQUEEZE routine, which removed 71 electrons per asymmetric unit, equivalent to approximately one hexane plus half a DCM molecule. The squeezed solvent content is added to the formula unit. These details are added to the SQF file appended to the CIF in the section: _platon_squeeze_details. Compound **3** crystallises in the monoclinic system, space group $P2_1/c$, with two independent molecules in the asymmetric unit (eight per unit cell). One of the molecules shows disorder involving the Cp* ligand and the boron cage, which was successfully resolved with occupancy ratios of 0.56:0.44. The CIF was edited accordingly, and no A- or B-level alerts remain. Some hydrogen atoms associated with the disordered boron cage could not be located but were included in the formula unit. Crystallographic data have been deposited with the Cambridge Crystallographic Data Center as supplementary publication no CCDC - 2501036 (**1**), 2353839 (**2**), and 2487781 (**3**). The data can be obtained free of charge from The Cambridge Crystallographic Data Centre via www.ccdc.cam.ac.uk/data_request/cif.

Crystal data for **1**: $C_{20}H_{49.73}B_{12.86}Ti_2$, M_r.= 525.20, triclinic, space group P-1, a = 12.4681(10) Å, b = 16.8148(13) Å, c = 21.8299(18) Å, α = 100.348(3)°, β = 95.369(3)°, γ = 104.634(3)°, V = 4309.5(6) Å^3, Z = 6, ρ_{calcd} = 1.214 g/cm^3, μ = 0.566 mm^{-1}, *F(000)* = 1668.0, R_1 = 0.0885, wR_2 = 0.2794, 13145 independent reflections [2θ ≤ 56.622°] and 1630 parameters.

Crystal data for **2**: $C_{26.50}H_{51}B_{15}ClSTi_2$, M_r.= 695.13, orthorhombic, space group $Pna2_1$, a = 28.441(3) Å, b = 9.5780(9) Å, c = 14.6840(13) Å, α = 90°, β = 90°, γ = 90°, V = 4000.0(6) Å^3, Z = 4, ρ_{calcd} = 1.154 g/cm^3, μ = 0.537 mm^{-1}, *F(000)* = 1448.0, R_1 = 0.1096, wR_2 = 0.2713, 5561 independent reflections [2θ ≤ 45.996°] and 386 parameters.

Crystal data for **3**: $C_{20}H_{48}B_{14}OSTi_2$, M_r.= 583.78, triclinic, space group $P2_1/c$, a = 18.9743(11) Å, b = 19.9731(12) Å, c = 18.6090(12) Å, α = 90°, β = 117.496(2)°, γ = 90°, V = 6255.7(7) Å^3, Z = 8, ρ_{calcd} = 1.240 g/cm^3, μ = 0.0.593 mm^{-1}, *F(000)* = 2448.0, R_1 = 0.0657, wR_2 = 0.1887, 9407 independent reflections [2θ ≤ 56.322°] and 1153 parameters.

II Computational Details

All molecular structures were fully optimized using the *Gaussian 16*[8] software package with the BP86 functional[9] and the def2-SVP basis set obtained from the EMSL Basis Set Exchange.[10] Geometry optimizations were carried out in the gas phase (no solvation model) starting from the corresponding X-ray crystallographic coordinates. For **1**, geometry optimizations were performed starting from both possible hydrogen arrangements shown in Figure S1. During the optimization, arrangement (b) converged to arrangement (a), which corresponds to the lowest-energy structure. Vibrational frequency calculations at the same level of theory confirmed that all optimized geometries correspond to true minima on the potential energy surface, as no imaginary frequencies were detected. Further, the gauge including atomic orbital (GIAO)[11-13] method was employed to compute the ^{11}B chemical shifts. The NMR chemical shifts were calculated using the hybrid Becke−Lee−Yang−Parr (B3LYP) functional[14] and the def2-TZVP basis set on the optimized geometries. The ^{11}B NMR chemical shifts were calculated relative to B_2H_6 (B3LYP B shielding constant 84.05 ppm) and converted to the usual [BF_3.OEt_2] scale using the experimental δ (^{11}B) value of B_2H_6, 16.6 ppm.[15] Natural Bond Orbital (NBO) analyses,[16] including the calculation of Wiberg bond indices (WBI)[17], were performed within the Gaussian 16 environment. To gain further insight into the bonding characteristics, the electron-density distribution (ρ) derived from the optimized wavefunctions was examined using the Quantum Theory of Atoms in Molecules (QTAIM).[18] The QTAIM analyses were carried out with the Multiwfn v3.4 program,[19] using wavefunctions generated at the same computational level as the geometry optimizations. All optimized structures and molecular orbital visualizations were prepared using Gaussview[20] and Chemcraft[21].

Table.S2. Selected geometrical parameters and Wiberg bond indices (WBI) of **1** and **2**.

1				**2**			
	Expt.	Cal.	WBI		Expt.	Cal.	WBI
Ti1-B1	2.339	2.353	0.456	Ti1-Ti2	3.246	3.234	0.362
Ti1-B5	2.414	2.443	0.276	Ti1-B3	2.61	2.521	0.308
Ti1-B9	2.407	2.451	0.274	Ti1-B4	2.33	2.423	0.374
Ti2-B5	2.244	2.229	0.406	Ti1-B10	2.58	2.623	0.277
Ti2-B6	2.411	2.443	0.396	Ti2-B14	2.35	2.288	0.583
Ti2-B7	2.334	2.356	0.442	Ti2-B1	2.43	2.586	0.253
Ti2-B9	2.247	2.218	0.414	Ti1-S1	2.309	2.527	0.713
B1-B2	1.844	1.878	0.488	B4-B14	1.85	1.670	0.736
B1-B5	1.840	1.881	0.575	B10-B11	1.91	1.791	0.545
B1-B6	2.021	1.940	0.464	B14-B15	1.75	1.829	0.460
B3-B4	1.840	1.881	0.479				
B6-B7	1.674	1.763	0.659				
B5-B9	1.795	1.800	0.554				

Table S3. Selected experimental and calculated bond angles of **1** and **2**.

1			**2**		
	Expt.	Cal.		Expt.	Cal.
Ti1-B5-Ti2	134.460	134.470	Ti1-B4-Ti2	81.90	84.414
B5-Ti1-B9	43.716	43.157	Ti1-Ti2-B4	45.26	48.212
B1-Ti1-B2	46.288	47.009	Ti1-B10-B11	121.90	121.973
B1-B5-B2	64.883	66.645	B11-B15-B12	64.00	61.536
B7-Ti2-B11	138.041	145.333	Ti1-S1-Ti2	90.98	80.403
B6-B7-B8	117.809	112.002			
Ti1-B1-B6	112.857	116.545			
B1-B6-B7	121.735	125.265			
B8-B9-B10	111.304	115.754			

Table S4. Calculated natural charges (q) and natural valence population (Pop) of **1** and **2**.

1			**2**		
	q	Pop(val)		q	Pop(val)
Ti1	-0.030	4.035	Ti1	0.326	3.691
Ti2	0.038	3.988	Ti2	0.382	3.637
B1	-0.133	3.113	B1	-0.263	3.242
B2	-0.142	3.122	B2	-0.201	3.180
B3	-0.130	3.110	B3	-0.239	3.215
B4	-0.140	3.120	B4	-0.257	3.232
B5	-0.304	3.270	B5	-0.255	3.224
B6	-0.201	3.179	B6	-0.095	3.062
B7	-0.107	3.082	B7	-0.133	3.101
B8	-0.194	3.172	B8	-0.218	3.0189
B9	-0.307	3.273	B9	-0.144	3.113
B10	-0.193	3.172	B10	-0.237	3.211
B11	-0.107	3.082	B11	-0.105	3.085
B12	-0.201	3.179	B12	-0.129	3.109
			B13	-0.077	3.050
			B14	-0.241	3.211
			B15	-0.215	3.190
			S1	-0.142	6.127

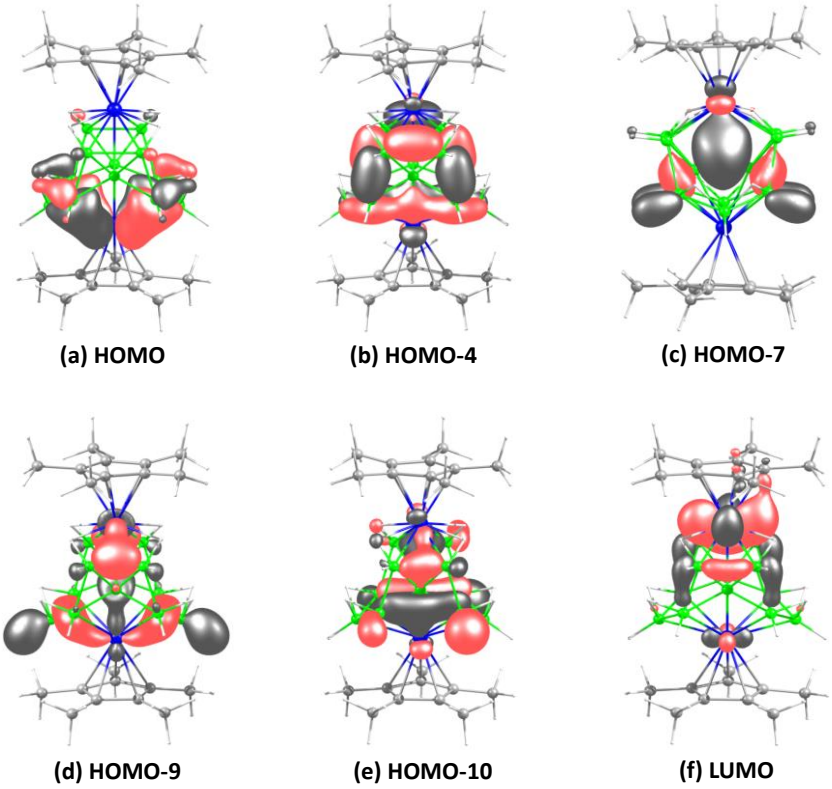

Figure S30. Selected molecular orbitals of **1** (isocontour values: ±0.045 [e.bohr^{-3}]$^{1/2}$).

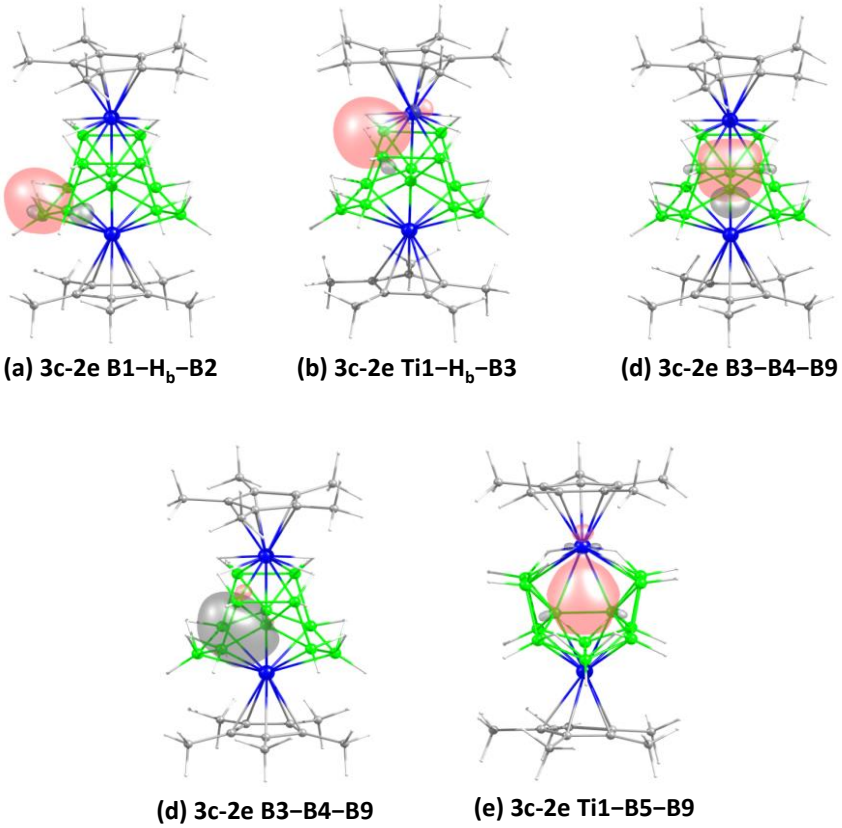

Figure S31. Selected NBO interactions of **1** (isocontour values: ±0.045 [e.bohr^{-3}]$^{1/2}$).

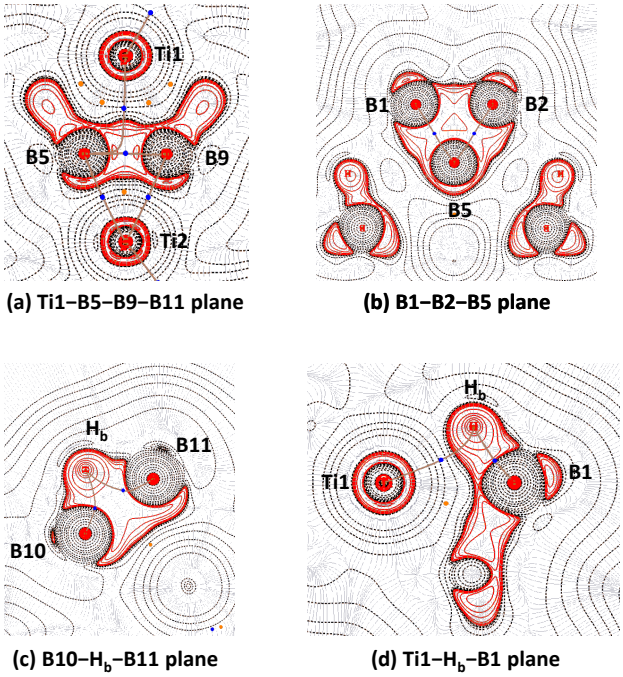

(a) Ti1–B5–B9–B11 plane (b) B1–B2–B5 plane

(c) B10–H_b–B11 plane (d) Ti1–H_b–B1 plane

Figure S32. Contour-line diagram of the Laplacian of the electron density of **1** in selected planes. The solid brown lines are bond paths, whereas blue dots indicate the bond-critical points (BCP). Solid red lines indicate the areas of charge concentration ($\nabla^2\rho(r) < 0$), while dashed black lines show the areas of charge depletion ($\nabla^2\rho(r) > 0$).

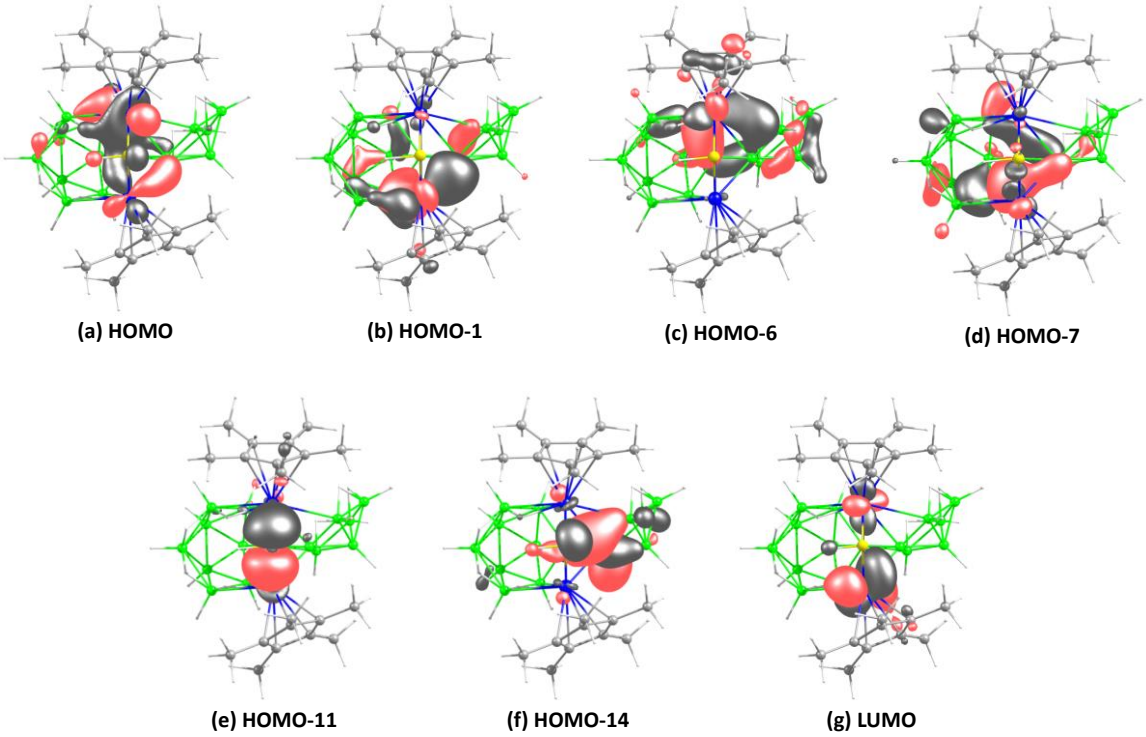

(a) HOMO (b) HOMO-1 (c) HOMO-6 (d) HOMO-7

(e) HOMO-11 (f) HOMO-14 (g) LUMO

Figure S33. Selected molecular orbitals of **2** (isocontour values: ±0.045 [e.bohr^{-3}]$^{1/2}$). The MO analyses showed that the HOMOs is delocalized over the d orbitals of two Ti centers, with additional Ti–B interactions extending into the cluster framework, whereas the LUMOs are primarily localized on the d orbitals of two Ti centers. The Wiberg bond index (WBI) of 0.362 suggests weak Ti–Ti bonding interactions. In addition, the analysis shows the existence of extended delocalized bonding interactions between the constituents of the clusters, observed in HOMO, HOMO-1, HOMO-6, HOMO-7, and HOMO-14. Additionally, NBO analysis confirms the bonding interactions throughout the cluster skeleton (Figure S33). The MO and NBO analyses further revealed distinct types of metal-boron interactions involving the triangular faces at the cluster fusion.

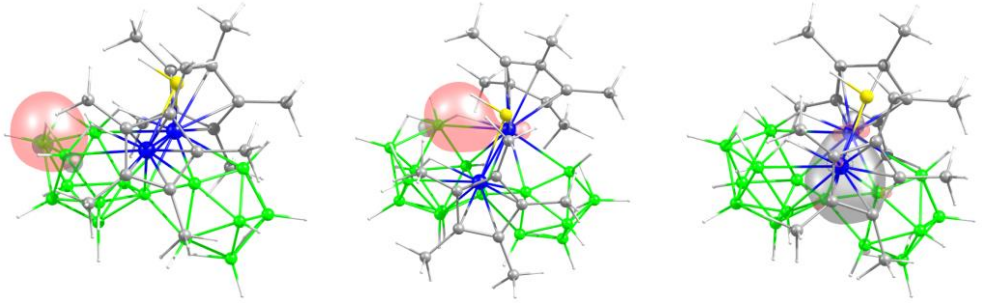

(a) 3c-2e B1–H_b–B2 (b) 3c-2e Ti1–H_b–B3 (c) 3c-2e Ti1–B4–B14

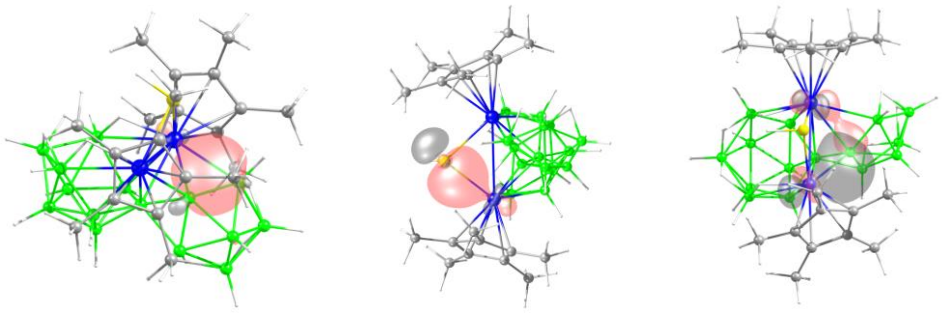

(d) 3c-2e Ti1–B10–B14 (e) 2c-2e Ti2–S1 (f) 3c-2e Ti1–B14–Ti2

Figure S34. Selected NBO interactions of **2** (isocontour values: ±0.045 [e.bohr^{-3}]$^{1/2}$).

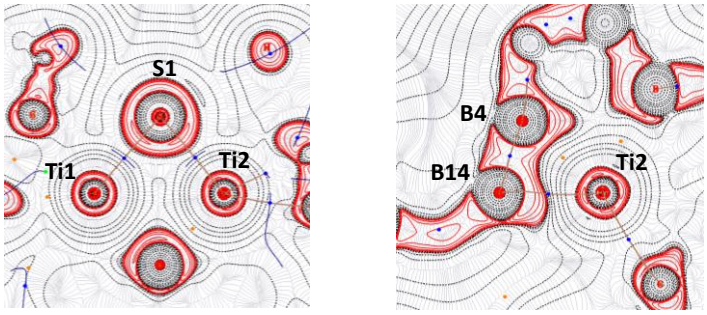

(a) Ti1–S1–Ti2 plane (b) Ti2–B14–B4 plane

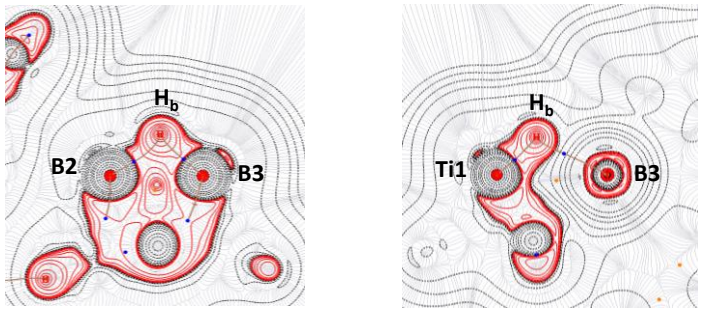

(c) B2–H_b–B3 plane (d) Ti1–H_b–B1 plane

Figure S35. Contour-line diagram of the Laplacian of the electron density of **2** in selected planes. The solid brown lines are bond paths, whereas blue dots indicate the bond-critical points (BCP). Solid red lines indicate the areas of charge concentration ($\nabla^2\rho(r) < 0$), while dashed black lines show the areas of charge depletion ($\nabla^2\rho(r) > 0$).

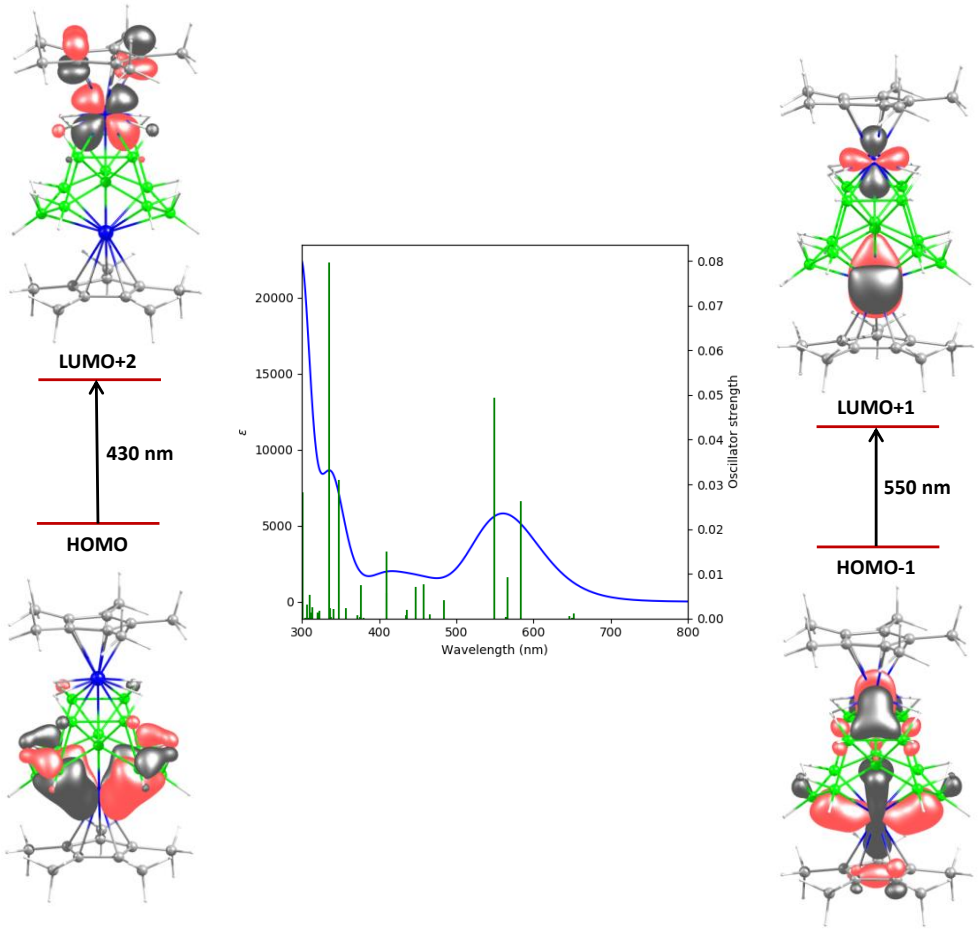

Figure S36. Absorption spectrum computed at TD-DFT-BP86/Def2-SVP level of theory (ε in $LM^{-1}cm^{-1}$) and selected molecular orbitals of **1** related to most intense electronic transitions [isocontour values: ±0.045 $(e/bohr^3)^{1/2}$].

Table S5. TD-DFT calculated energies (excitation energy (eV), λ_{calc} (nm)), oscillator strength (*f*), and main composition of the first UV−vis electronic excitations for **1**. Experimental absorption wavelengths (λ_{exp}, nm) of **1** are given for comparison.

No	Excitation Energy (eV)	Wavelength λ (nm)		Main electronic transition (% weight) [b]
		Calc. (*f*) [a]	Expt.	
1	2.124	584 (0.026)		HOMO-1→LUMO (56)
				HOMO-1→LUMO+1 (30)
2	2.257	549 (0.049)	550	HOMO-1→LUMO (24)
				HOMO-1→LUMO+1 (55)
3	3.030	409 (0.015)	430	HOMO→LUMO+2 (81)
4	3.563	348 (0.031)		HOMO-7→LUMO+1 (75)
5	3.699	335 (0.080)		HOMO-9→LUMO (50)

[a]Oscillator strength greater than 0.010 and [b]Components with greater than 20% contribution shown.

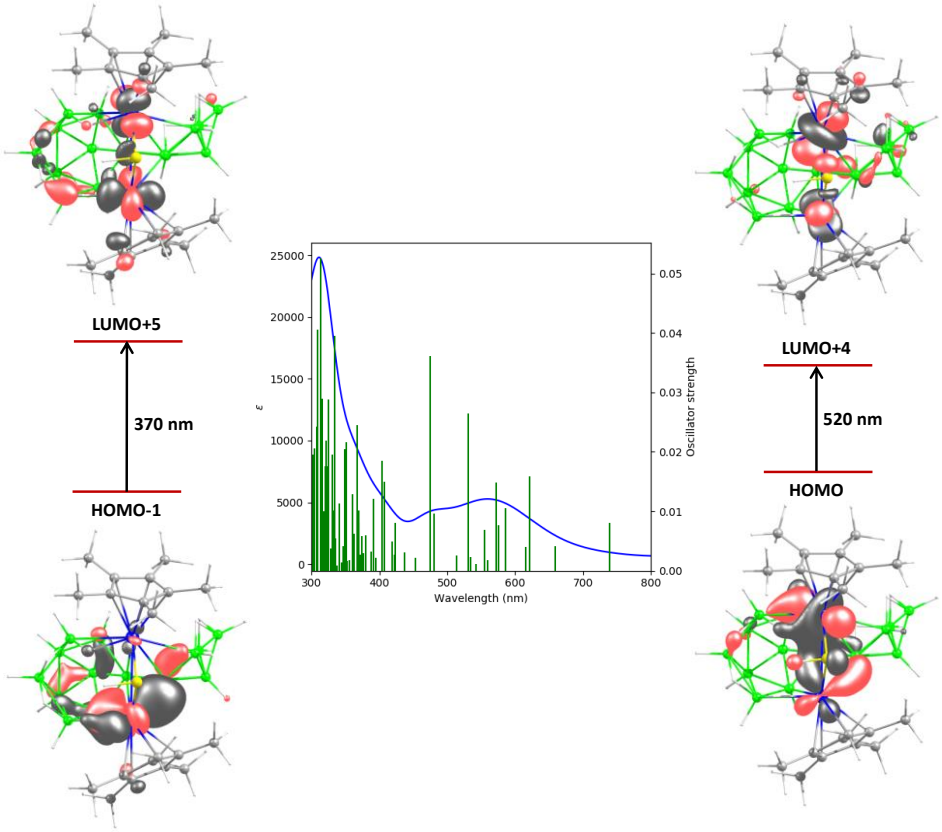

Figure S37. Absorption spectrum computed at TD-DFT-BP86/Def2-SVP level of theory (ε in $LM^{-1}cm^{-1}$) and selected molecular orbitals of **2** related to most intense electronic transitions [isocontour values: ±0.045 $(e/bohr^3)^{1/2}$].

Table S6. TD-DFT calculated energies (excitation energy (eV), λ_{calc} (nm)), oscillator strength (*f*), and main composition of the first UV–vis electronic excitations for **2**. Experimental absorption wavelengths (λ_{exp}, nm) of **2** are given for comparison.

No	Excitation Energy (eV)	Wavelength λ (nm)		Main electronic transition (% weight) [b]
		Calc. (*f*) [a]	Expt.	
1	1.997	621 (0.016)		HOMO-2→LUMO (82)
2	2.168	572 (0.015)		HOMO→LUMO+3 (73)
3	2.335	531 (0.026)	520	HOMO→LUMO+4 (76)
4	2.614	474 (0.036)		HOMO→LUMO+5 (69)
5	3.045	407 (0.015)		HOMO→LUMO+8 (61)
6	3.074	403 (0.018)		HOMO-1→LUMO+4 (64)
7	3.373	368 (0.025)	370	HOMO→LUMO+9 (16)
				HOMO-1→LUMO+5 (29)
				HOMO-3→LUMO+3 (15)
8	3.530	351 (0.022)		HOMO→LUMO+10 (20)
				HOMO-4→LUMO+4 (33)
9	3.557	349 (0.020)		HOMO-4→LUMO+4 (26)
				HOMO-9→LUMO (38)
10	3.717	334 (0.040)		HOMO-1→LUMO+6 (21)
				HOMO-5→LUMO+4 (22)

[a]Oscillator strength greater than 0.015 and [b]Components with greater than 15% contribution shown.

III Cartesian Coordinates of all Optimized Structures

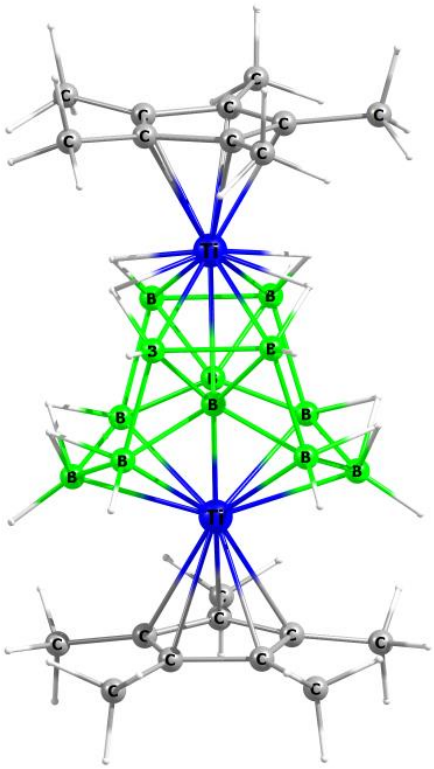

Figure S38. Optimized geometry of **1**.

Total energy = -2787.60283462 a.u.

Cartesian coordinates for the calculated structure **1** (in Å)

C	4.180510000	0.899099000	0.791076000
C	4.145001000	-0.496505000	1.148575000
C	4.092222000	-1.261395000	-0.065739000
C	4.167061000	-0.352990000	-1.175927000
C	4.193162000	0.987335000	-0.648673000
C	-4.246483000	-0.016784000	-1.223846000
C	-4.233302000	-1.201027000	-0.401712000
C	-4.251491000	-0.780863000	0.971913000
C	-4.285098000	0.661372000	0.999807000
C	-4.287110000	1.134231000	-0.356355000
B	0.829168000	-1.331148000	-1.517299000
H	1.393066000	-2.368635000	-1.800549000
B	1.389745000	0.186550000	-2.249545000
H	2.101112000	0.249738000	-3.228774000
B	0.766090000	1.599913000	-1.399441000
H	1.294924000	2.680309000	-1.564223000
B	0.757716000	1.503713000	1.491036000
H	1.286238000	2.570531000	1.728923000
B	1.377913000	0.036533000	2.247530000
H	2.088504000	0.034674000	3.229655000
B	0.820585000	-1.428911000	1.413224000
H	1.384648000	-2.483000000	1.628037000
B	-1.086597000	1.875711000	-0.886908000
H	-1.294462000	3.028274000	-1.198301000
B	-1.006625000	-1.807945000	0.871561000
H	-1.175166000	-2.962868000	1.200523000
B	-1.091316000	1.810191000	0.990457000
H	-1.310868000	2.932417000	1.394111000
B	-1.002321000	-1.748910000	-1.008588000
H	-1.158259000	-2.886370000	-1.396382000
B	0.028896000	0.953769000	0.023256000
B	0.076171000	-0.844745000	-0.037034000
Ti	2.085779000	0.094169000	0.001258000
Ti	-2.222720000	0.005900000	-0.011084000
C	4.390092000	-1.088184000	2.509303000
H	3.705462000	-1.931255000	2.732701000
H	5.429541000	-1.483553000	2.562932000
H	4.278246000	-0.340847000	3.316945000
C	4.355143000	2.054669000	1.740195000
H	5.434794000	2.279204000	1.895162000
H	3.880622000	2.980246000	1.357587000
H	3.909984000	1.845096000	2.732407000
C	4.371290000	2.251206000	-1.447329000
H	5.450471000	2.505835000	-1.550633000
H	3.949621000	2.157319000	-2.467123000
H	3.875975000	3.118702000	-0.967058000
C	4.445180000	-0.769126000	-2.593889000
H	4.318564000	0.065982000	-3.308112000
H	5.497479000	-1.123140000	-2.678862000
H	3.790303000	-1.599255000	-2.926934000
C	4.135224000	-2.762844000	-0.155467000
H	3.671315000	-3.132751000	-1.091047000

H	5.186146000	-3.131699000	-0.137937000
H	3.604689000	-3.241256000	0.691681000
C	-4.442911000	2.565689000	-0.787106000
H	-4.012172000	2.746235000	-1.790854000
H	-5.520294000	2.841805000	-0.832205000
H	-3.946753000	3.263790000	-0.085301000
C	-4.454799000	1.518458000	2.224657000
H	-3.973530000	2.508718000	2.105812000
H	-5.535128000	1.693976000	2.425322000
H	-4.025829000	1.043604000	3.128956000
C	-4.380371000	-1.691162000	2.163048000
H	-3.962969000	-1.236555000	3.083086000
H	-5.452007000	-1.914572000	2.362823000
H	-3.863904000	-2.657459000	2.002229000
C	-4.320185000	-2.621004000	-0.886428000
H	-3.776925000	-3.317862000	-0.219032000
H	-5.381967000	-2.952388000	-0.928676000
H	-3.894974000	-2.739163000	-1.901691000
C	-4.346938000	0.011109000	-2.725880000
H	-5.413758000	0.002150000	-3.042362000
H	-3.885612000	0.921310000	-3.157557000
H	-3.859752000	-0.867786000	-3.192421000
H	0.438847000	-0.942298000	2.566852000
H	0.405624000	0.958019000	2.625640000
H	0.417133000	1.130563000	-2.568163000
H	0.451319000	-0.768654000	-2.636709000
H	-1.879776000	1.131564000	-1.530036000
H	-1.835541000	-1.003862000	-1.596636000
H	-1.841877000	-1.094279000	1.497028000
H	-1.884706000	1.016606000	1.572761000

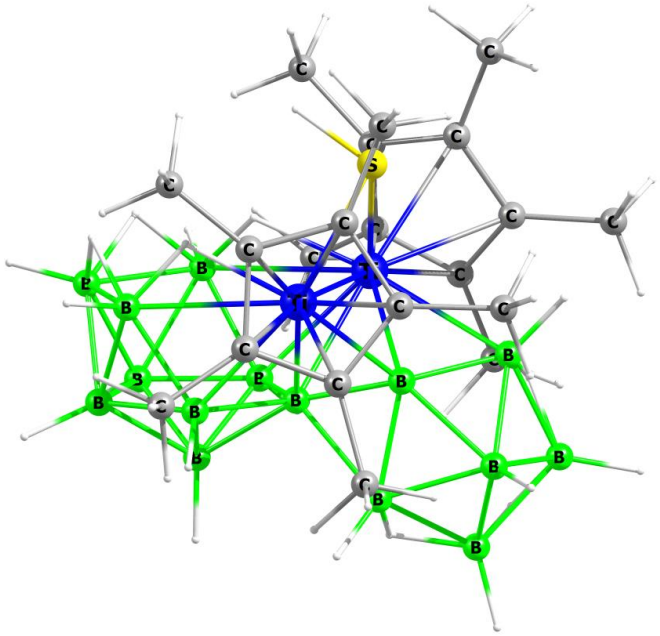

Figure S39. Optimized geometry of **2**

Total energy = -3262.02854610 a.u.

Cartesian coordinates for the calculated structure **2** (in Å)

Ti	-1.714933000	-0.128570000	-0.218378000
Ti	1.516889000	-0.090806000	-0.093358000
C	-4.112845000	-0.204340000	0.023335000
C	-3.642440000	0.965516000	0.713339000
C	-3.060134000	1.855363000	-0.256285000
C	-3.187650000	1.236397000	-1.551329000
C	-3.812897000	-0.045881000	-1.375841000
C	-4.962315000	-1.293400000	0.617567000
H	-4.764550000	-2.280545000	0.156649000
H	-4.798918000	-1.397772000	1.707093000
H	-6.040312000	-1.061665000	0.463110000
C	-3.865909000	1.251836000	2.171752000
H	-3.176980000	2.027773000	2.553383000
H	-4.906064000	1.612687000	2.336468000
H	-3.730257000	0.347863000	2.798076000
C	-2.571662000	3.257204000	-0.017934000
H	-2.270456000	3.416782000	1.034124000
H	-1.698100000	3.504693000	-0.654200000
H	-3.370600000	3.995504000	-0.256102000
C	-2.919193000	1.906720000	-2.870833000
H	-2.085544000	2.632790000	-2.810796000
H	-2.669168000	1.179630000	-3.669470000
H	-3.824846000	2.461294000	-3.206116000
C	-4.257369000	-0.968816000	-2.479294000
H	-4.288903000	-2.025102000	-2.147181000
H	-5.281110000	-0.702119000	-2.825929000
H	-3.591683000	-0.912827000	-3.364387000
C	3.831771000	0.482435000	0.426525000
C	3.870162000	-0.735907000	-0.328880000
C	3.375076000	-0.440517000	-1.651484000
C	3.080957000	0.965241000	-1.715854000
C	3.376942000	1.544573000	-0.439979000
C	4.423432000	0.630256000	1.803418000
H	4.026504000	-0.122721000	2.515700000
H	5.525607000	0.477791000	1.764536000
H	4.257108000	1.637524000	2.233132000
C	4.591814000	-1.973856000	0.128393000
H	4.585961000	-2.767747000	-0.640948000

H	5.655945000	-1.728407000	0.343361000
H	4.159104000	-2.401513000	1.056225000
C	3.395204000	-1.359266000	-2.842940000
H	2.546544000	-1.166477000	-3.530784000
H	4.328005000	-1.211308000	-3.431678000
H	3.352507000	-2.424531000	-2.547319000
C	2.773865000	1.744622000	-2.963856000
H	2.275076000	1.124208000	-3.733788000
H	2.117652000	2.614694000	-2.765521000
H	3.716591000	2.131939000	-3.413386000
C	3.534441000	3.022898000	-0.206839000
H	2.746823000	3.616295000	-0.709468000
H	3.526272000	3.300200000	0.864780000
H	4.513606000	3.356511000	-0.618935000
B	-1.604629000	-1.952266000	1.268147000
H	-2.622688000	-1.815565000	1.916076000
B	-1.811669000	-2.709052000	-0.366092000
H	-2.863226000	-3.246908000	-0.657588000
B	-1.024411000	-3.594272000	1.112661000
H	-1.647856000	-4.581220000	1.430790000
B	-0.128783000	-3.853000000	-0.500038000
B	0.738506000	-3.567447000	1.096037000
H	1.378036000	-4.539120000	1.431054000
B	1.419770000	-2.597096000	-0.351705000
B	1.300552000	-1.907805000	1.315596000
H	2.306221000	-1.745254000	1.992712000
B	-0.161377000	-2.516501000	2.171034000
B	0.656075000	1.268589000	3.939511000
B	1.418102000	2.451272000	2.838029000
H	1.928978000	3.476759000	3.221312000
B	0.818912000	2.088068000	1.189501000
B	-0.242638000	0.774025000	1.282578000
B	-0.445387000	0.254739000	2.947114000
B	-0.251310000	2.007446000	2.633817000
H	-1.119785000	2.819684000	2.857775000
B	-0.175748000	-0.886728000	1.447187000
S	-0.075688000	0.702624000	-1.888306000
H	-0.084565000	-5.002071000	-0.885279000
H	2.441597000	-3.094305000	-0.759558000
H	-0.180423000	-2.695286000	3.368760000
H	1.950240000	1.436882000	3.591032000
H	0.564303000	1.453850000	5.128696000
H	-1.375916000	-0.172120000	3.588128000
H	2.032536000	1.945939000	1.744646000
H	0.687058000	-0.035171000	3.663872000
H	-0.146976000	-0.321758000	-2.795445000
H	1.032673000	-1.582029000	-1.078475000
H	0.639978000	-3.235249000	-1.341374000
H	-1.062935000	-3.359111000	-1.299677000
H	-1.665375000	-1.736583000	-1.194695000
H	0.842932000	3.031183000	0.432921000

References

1 G. H. Llinás, M. Mena, F. Palacios, P. Royo and R. Serrano, *J. Organomet. Chem.*, 1988, **340**, 37.

2 P. Govindaswamy, Y. A. Mozharivskyj, M. R. Kollipara, *Polyhedron* 2005, **24**, 1710.

3 (a) C. E. Rao, S. K. Barik, K. Yuvaraj, K. Bakthavachalam, T. Roisnel, V. Dorcet, J.-F. Halet, Ghosh, *Eur. J. Inorg. Chem.* **2016**, 4913; (b) A. Haridas, S. Kar, B. Raghavendra, T. Roisnel, V. Dorcet, S. Ghosh, *Organometallics* 2020, **39**, 58.

4 (a) S. Bairagi, A. N. Pradhan, M. Cordier, T. Roisnel and S. Ghosh, *Eur. J. Inorg. Chem.,* 2023, **26**, e202300060; (b) S. Bairagi, D. K. Patel, D. Chatterjee, M. Kučeráková, J. Macháček, T. Base, T. Pradeep and S. Ghosh, *Chem. Sci.*, 2025, **16**, 14127; (c) S. Bairagi, S. Giri, G. Joshi, E. D. Jemmis and S. Ghosh, *Angew. Chem. Int. Ed.*, 2024, e202417170; (d) S. Bairagi, D. Chatterjee, S. Giri and S. Ghosh, *Chem. Commun.*, 2025, **61**, 3696.

5 A. Altomare, G. Cascarano, C. Giacovazzo, A. Guagliardi, M. C. Burla, G. Polidori and M. Camalli, *J. Appl. Crystallogr*., 1994, **27**, 435.

6 G. M. Sheldrick, *Acta Cryst.*, 2015, **C71**, 3.

7 O. V. Dolomanov, L. J. Bourhis, R. J. Gildea, J. A. K. Howard and H. Puschmann, *J. Appl. Cryst*., 2009, **42**, 339.

8 Gaussian 16, Revision B.01, M. J. Frisch, G. W. Trucks, H. B. Schlegel, G. E. Scuseria, M. A. Robb, J. R. Cheese-man, G. Scalmani, V. Barone, G. A. Petersson, H. Nakatsuji, X. Li, M. Caricato, A. V. Marenich, J. Bloino, B. G. Janesko, R. Gomperts, B. Mennucci, H. P. Hratchian, J. V. Ortiz, A. F. Izmaylov, J. L. Sonnenberg, D. Williams-Young, F. Ding, F. Lip- parini, F. Egidi, J. Goings, B. Peng, A Petrone, T. Henderson, D. Ranasinghe, V. G. Zakrzewski, J. Gao, N. Rega, G. Zheng, W. Liang, M. Hada, M. Ehara, K. Toyota, R. Fukuda, J. Hasegawa, M. Ishida, T. Nakajima, Y. Honda, O. Kitao, H. Nakai, T. Vreven, K. Throssell, J. A. Jr. Montgomery, J. E. Peralta, F. Ogliaro, M. J. Bearpark, J. J. Heyd, E. N. Brothers, K. N. Kudin, V. N. Staroverov, T. A. Keith, R. Kobayashi, J. Normand, K. Raghavachari, A. P. Rendell, J. C. Burant, S. S. Iyengar, J. Tomasi, M. Cossi, J. M. Millam, M. Klene, C. Adamo, R. Cammi, J. W. Ochterski, R. L. Mar- tin, K. Morokuma, O. Farkas, J. B. Foresman, D. J. Fox, Gaussian, Inc., Walling- ford CT, 2016.

9 (a) H. L. Schmider, A. D. Becke, *J. Chem. Phys.* 1998, **108**, 9624; (b) J. P. Perdew, *Phys. Rev. B: Condens. Matter Mater. Phys.* 1986, **33**, 8822.

10 EMSL Basis Set Exchange Library. https://bse.pnl.gov/bse/portal

11 F. London, *J. Phys. Radium*., 1937, **8**, 397.

12 R. Ditchfield, *Mol. Phys.*, 1974, **27**, 789.

13 K. Wolinski, J. F. Hinton and P. Pulay, *J. Am. Chem. Soc.*, 1990, **112**, 8251.

14 (a) A. D. Becke, *Phys. Rev. A.*, 1988, **38**, 3098; (b) C. Lee, W. Yang and R. G. Parr, *Phys. Rev. B.*, 1988, **37**, 785; (c) A. D. Becke, *J. Chem. Phys.*, 1993, **98**, 5648.

15 T. P. Onak, H. L. Landesman, R. E. Williams and I. Shapiro, *J. Phys.Chem.*, 1959, **63**, 1533.

16 (a) E. D. Glendening, A. E. Reed, J. E. Carpenter and F. Weinhold, *NBO Program 3.1*, W. T. Madison, 1988; (b) A. E. Reed, F. Weinhold and L. A. Curtiss, *Chem. Rev.*, 1988, **88**, 899; (c) F. Weinhold and R. Landis, *Valency and bonding: A natural bond orbital donor-acceptor perspective;* Cambridge University Press: Cambridge, U.K, 2005.

17 K. Wiberg, *Tetrahedron*, 1968, **24**, 1083.

18 (a) R. F. W. Bader, *Atoms in Molecules: A Quantum Theory*; Oxford University Press: Oxford, U. K., 1990; (b) R. F. W. Bader, *J. Phys. Chem. A.*, 1998, **102**, 7314; (c) R. F. W. Bader, *Chem. Rev.*, 1991, **91**, 893.

19 T. Lu, F. Chen, *J. Comput. Chem.*, 2012, **33**, 580.

20 I. I. Dennington, R. T. Keith, J. Millam, K. Eppinnett, W. L. Hovell and R. Gilliland, *GaussView, Version 3.09*; Semichem Inc.: Shawnee Mission, KS, 2003.

21 G. A. Zhurko, http://www.chemcraftprog.com.